



ELSEVIER

Contents lists available at [ScienceDirect](https://www.sciencedirect.com)

Journal of the Mechanics and Physics of Solids

journal homepage: www.elsevier.com/locate/jmps

Dispersion and attenuation relations in flexoelectricity

Antonios E. Giannakopoulos^{a,*}, Ares J. Rosakis^b^a *Mechanics Division, National Technical University of Athens, Greece*^b *Graduate Aerospace Laboratory, California Institute of Technology, Pasadena CA 91125 USA*

ARTICLE INFO

Keywords:

Flexoelectricity
Plane waves
Dispersion curves
Flexoelectric metamaterials

ABSTRACT

The dispersion relations in flexoelectricity are examined for plane time-harmonic waves that propagate in the flexoelectric materials. In contrast to classic elastodynamics, dispersion is observed in the displacement field due to two micro-structural and two micro-inertial lengths that emerge from the electromechanical coupling. In the absence of such coupling, we return to the classic elastodynamic results. The problem dissociates in longitudinal and transverse waves, as is the case in classic elastodynamics. The group velocity of the mechanical field is also the velocity of the energy transfer across the planes of the waves. An optical branch of the dispersion relation appears due to the polarization field that follows the mechanical field. The longitudinal and transverse velocities of the plane waves was found to depend on the corresponding microstructural lengths and are less than or equal to the classic plane wave velocities because the micro-inertial lengths are greater than or equal to the micro-structural length. The opposite effect is expected when we encounter flexoelectric metamaterials in which case the micro-inertial lengths are less than the micro-structural length.

1. Introduction

Flexoelectricity is the ability of materials to convert mechanical strain gradients to electric polarization and vice versa. However, an electric field that changes with time gives rise to a magnetic field that also has to be accounted for, through Maxwell-Ampere law. Many rocks that comprise earth's exhibit flexoelectricity, often combined with piezoelectricity (in cases when anisotropy is present). An excellent recent perspective of this unusual electromechanical coupling with emphasis on applications in energy harvesting, micro-electro-mechanical systems, nanotechnology and biology can be found in [Krichen and Sharma \(2016\)](#) as well as other review very informative articles like [Tagantsev \(1991\)](#), [Yudin and Tagantsev \(2013\)](#), [Zubko et al. \(2007\)](#), [Wang et al. \(2019\)](#) to mention but few.

Modeling of flexoelectricity requires several material parameters, and for most materials these have not been measured yet. Experimental methods fall into two major categories: (a) vibration of structural components (e.g. beams, rods, plates), [Ma and Cross \(2006\)](#), [Zubko et al. \(2007\)](#) and references therein and (b) wave dispersion curves (i.e. neutron scattering), [Axe et al. \(1970\)](#), [Harada et al. \(1971\)](#), [Shirane et al. \(1970\)](#), [Yamada and Shirane \(1969\)](#), [Stirling \(1972\)](#) and others. The experimental measurements often differ in magnitude and sign. Structural components have surfaces that contribute to the flexoelectric phenomenon, as predicted by [Tagantsev \(1991\)](#) and pointed out by [Maranganti and Sharma \(2009\)](#). The role of surface in flexoelectricity has since been examined thoroughly, see for example [Stengel \(2016\)](#) and [Mizzi et al. \(2022\)](#). On the other hand, neutron scattering and other methods do not suffer from the influence of the surface effects. The dispersion curves depend on temperature ([Shirane et al., 1967](#)), as well as on

* Corresponding author.

E-mail address: agiannak@uth.gr (A.E. Giannakopoulos).<https://doi.org/10.1016/j.jmps.2024.105648>

Received 24 January 2024; Received in revised form 8 April 2024; Accepted 12 April 2024

Available online 13 April 2024

0022-5096/© 2024 Elsevier Ltd. All rights reserved.

pressure (Coak et al., 2019), having a direct influence on the dielectric susceptibility. Therefore, we expect the flexoelectric properties to depend on temperature and to some extent on pressure.

Aside from the experimental assessment, the flexoelectric properties can be estimated theoretically by several methods. The simplest method uses a rigid-ion model for lattice dynamics, Tagantsev (1991). Askar et al. (1970), on the other hand, used shell-type lattice-dynamical model to capture frequency dispersion. The later method extends to non-ionic materials. More recent methods use *ab initio* and empirical shell-models, following the pioneering work of Maraganti and Sharma (2009), see for example Xu et al. (2013). Note that such models do not account the surface influence, but apply to 0 K temperatures.

Early approaches on flexoelectric dispersion relations can be found in Hu et al. (2018) who examined the uniaxial rod case. Recently, dispersion analyses of flexoelectric wave guides have been conducted for extension of rods by Qu et al. (2021a), and for torsion of rectangular rods by Qu et al. (2021b). Several works that utilize directly the dispersion curves from bulk waves can be found in the literature, as for example Kvasov and Tagantsev (2015) and Morozovska et al. (2016). These works present more complex models that include the flexodynamic tensor, the elastic strain gradients and other nonlinearities such as electrostriction. A common aspect of these works is that they apply to one dimensional wave propagations problems in the absence of boundaries.

In actual applications, boundary conditions are necessary and must be provided. Also, different waves may appear simultaneously, as for example in dynamic fracture (Giannakopoulos and Rosakis, 2020). Mello et al. (2010) investigated the near ground motion signatures associated with sub-Rayleigh and supershear ruptures using the laboratory earthquake experiments with Homalite specimens (a flexoelectric polymer). Elastic waves can be separated into dilatational and shear parts, each governed by an appropriate wave speed. The general spectral representation of such waves can be given by inverse Fourier transforms where the plane wave propagation vectors are related to the dispersion relations. It is then important to have analytical expressions of the wavenumbers as functions of frequencies in order to construct the impulse response functions analytically. Various continuum flexoelectric theories have been proposed (for a recent review see Codony et al., 2021) but unfortunately involve numerous parameters which make their implementation cumbersome. However, the difficulties encountered in dynamic fracture mechanics require a moderately complex flexoelectric theory still capturing the essential physics, such as the one used in this work.

The scope of this work is two-fold. First, to formulate a simple continuum dynamic flexoelectric model that can be utilized at moderate frequencies and wave numbers. To establish the dominant physical effects we will make a wave hierarchy as suggested by Whitham (1974). In this respect we introduce length scales to establish the dominance of the wave operations. Such a model can be utilized to investigate measured laboratory scaled seismic Fourier amplitude spectra, Mello et al. (2014). Second, to provide a simple methodology for obtaining flexoelectric properties using experimental dispersion curves and at the same time assess the ability of the dynamic model in the essential dispersion characteristics.

In this work, flexoelectricity is considered to be the only source of strain gradient effects, and the coupling of the mechanical problem is analogous to a problem of couple stress elasticity where the two characteristic types of lengths emerge as a combination of mechanical, dielectric and flexoelectric constants, Giannakopoulos and Rosakis (2020). The first type of length resembles the (well known in the context of couple stress elasticity) microstructural length which is connected to the displacement curvature (see also the anti-plane problem in static form by Gavardin et al., 2018 and in dynamic form by Giannakopoulos and Zisis (2019, 2020). The second type of length is less referenced (and hardly considered in metrology) and resembles the micro-inertial length which essentially introduces a non-classic kinetic energy term that connects to the micro-rotations of the matter. As will be shown, these micro-lengths create dispersion of plane waves, in contrast with classic elasto-dynamics that predict no such dispersion. Therefore, these dispersion relations are fundamentally different than the geometrically related dispersion encountered in wave guides such as circular cylinders, plates etc. that show dispersion in the context of classical elastodynamics (see for example Achenbach (1990), and prestressed hyperelasticity, Kaplunov et al. (2000)). Resemblance with our present investigation can be found in works related to composites, Ben-Amoz (1976), Santoza and Symes (1991), Wang and Sun (2002); theories of microstructured materials, Georgiadis et al. (2004), Gouriotis and Georgiadis (2017), Engelbrecht et al. (2005), Papargyri-Beskou et al. (2009); and ferroelectrics, Pauget and Maugin (1980), to mention few.

The present paper is structured as follows. Section 2 provides the basic mechanical and polarization field equations and corresponding boundary conditions. Section 3 performs the dispersion analysis for the mechanical and the optical cases separately, giving the corresponding dispersion relations between the frequency and the wave numbers. The necessary conditions to use separation of variables in the wave forms are discussed in Appendix A. The phase velocities and the group velocities are found in closed forms. The group velocities are proven to be energy and wavelength transport velocities in Appendices B and C. Section 4 gives the wave numbers as functions of the frequency. The analysis shows that two of the four wavenumbers of the dispersion analysis are imaginary. Section 5 provides a methodology to obtain flexoelectric properties from experimental dispersion curves and gives comparisons with available experimental results. Section 6 gives the analysis of plane waves in an infinite flexoelectric body. Section 7 gives a brief account of flexoelectric metamaterials and the analogy with viscoelasticity. Finally, Section 8 concludes with the basic findings of the work.

2. Flexoelectricity: the mechanical and the polarization fields

We examine a homogeneous, centrosymmetric, linear flexoelectric solid (being dielectric at the same time) with an energy density due to elastic deformation and electric polarization which depends on the strain gradients. Reverse flexoelectricity implies that the gradient of the polarization produces strain and should be included in the energy density. The elastic strain energy due to strain gradient effects will not be considered and the kinetic strain energy will not include micro-rotational effects.

In what follows, consider the flexo-electric problem with unknowns the material displacement vector u_i [m], the material (electric) polarization vector P_i [C/m^2] and the electric field E_i [Nm/C]. These are functions of the (right-handed) Cartesian coordinates

x_1, x_2, x_3 and the time t . The linear internal (Helmholtz) energy density function that includes deformation and polarization is (Mindlin, 1968; Maraganti et al., 2006; Liu et al., 2014; Sharma et al., 2010; Hu et al., 2018):

$$W = \left[\begin{aligned} &\frac{1}{2}a_{ij}P_iP_j + \frac{1}{2}b_{ijkl}P_{j,i}P_{l,k} + \frac{1}{2}c_{ijkl}\varepsilon_{ij}\varepsilon_{kl} + e_{ijkl}P_{j,i}\varepsilon_{kl} \\ &+ f_{ijkl}P_i\varepsilon_{kl,j} + b_{ij}^0P_{j,i} \end{aligned} \right] \quad (2.1)$$

The mechanical linear strain is related to the displacement vector as $\varepsilon_{ij} = (u_{i,j} + u_{j,i})/2$. $P_{i,j}$ is the gradient of the polarization vector P_i and $\varepsilon_{i,j,k}$ are the gradients of the strains. Repeated indices imply summation from 1 to 3 and $(\cdot)_{,i} = \partial/\partial x_i$. The dielectric body will be assumed to be a perfect insulator, so the divergence of the polarization vector is equal to minus the bounded charge inside the body, $\nabla \cdot \vec{P} = -\rho_{\text{bound}} [\text{C}/\text{m}^3]$. The compatibility equations are identical to classic linear elasticity. The form of the energy density function (2.1) omits an extra term that ensures thermodynamic stability of the total energy ($1/2 g_{ijklmn} u_{i,jk} u_{l,mn}$). This term represents the contribution of purely elastic nonlocal effects. This energy addition may stabilize the problems in the case that the microstructural lengths ℓ_p, ℓ_s defined below in Eqs. (2.30) and (2.31) are not real and positive, something that has not been experimentally observed so far. As has been found however (see Maraganti et al. (2006), erratum), for most problems, excluding this contribution is generally not important. Stengel (2016) has investigated the strain gradient elasticity in the context of flexoelectricity with ab initio formulation and found negative g_{ijklmn} , something not acceptable in the absence of flexoelectricity.

The material constants are: the elastic constant tensor c_{ijkl} [N/m^2], the direct (static) flexo-electric coefficient tensor f_{ijkl} [Nm/C], the reciprocal dielectric susceptibility tensor a_{ij} [Nm^2/C^2], the inverse flexo-electric coefficient tensor e_{ijkl} [Nm/C] and the gradient polarization coupling tensor b_{ijkl} [Nm^4/C^2]. The symmetries of the above constants have been addressed in Shu et al. (2011). All these material tensors should be positive definite. The constants b_{ij}^0 are related to the surface energy per unit area $T_s = (n_i b_{ij}^0 P_j)/2$ with n_i being the unit normal vector pointing outside the flexoelectric body (Mindlin, 1968) and do not affect the balance laws, but only the boundary conditions.

In the works on continuum flexoelectricity so far, the Maxwell electric self-field E_i was stated by an electric potential as $E_i = -\Phi_{,i}$ [N/C]. The total electric enthalpy is (Toupin, 1956):

$$\bar{H} = W - \frac{1}{2}\varepsilon_0 E_i E_i - E_i P_i = W - \frac{1}{2}\varepsilon_0 \Phi_{,i} \Phi_{,i} + \Phi_{,i} P_i \quad (2.2)$$

where, $\varepsilon_0 \approx 8.854 \times 10^{-12} \text{C}^2 \text{N}^{-1} \text{m}^{-2}$ [$= \text{Fm}^{-1}$] is the dielectric permittivity of vacuum (assumed to surround the body). The energy density is the sum of the internal energy and the energy of the Maxwell self-field: $W + (1/2)\varepsilon_0 \Phi_{,i} \Phi_{,i}$.

The kinetic energy density is:

$$T = \frac{1}{2} \rho \dot{u}_i \dot{u}_i \quad (2.3)$$

where ρ is the material mass density and $\dot{u}_i = \partial u_i / \partial t$ is the material velocity vector. If $\rho = 0$, the problem reduces to the static case. Note that in this approach, we neglect the kinetic energy of the oscillations of the ions $\dot{P}_i \dot{P}_i m / (2ne^2) = \dot{P}_i \dot{P}_i \gamma / 2$, where m is the effective mass of the ions, n is the number of ions per unit volume and e is the effective charge of the ions in the dielectric and γ [kgm^3/C^2] is the polarization inertia. We will discuss more about the kinetic energy density in Section 5.

Accordingly, the constitutive equations are written as: a. Cauchy (symmetric) stress tensor:

$$\sigma_{ij} = \frac{\partial W}{\partial \varepsilon_{ij}} = c_{ijkl} \varepsilon_{kl} + e_{kl ij} P_{l,k} \quad (2.4)$$

b. Dipolar stress tensor:

$$\tau_{ijk} = \frac{\partial W}{\partial \varepsilon_{jki}} = f_{ijk} P_l \quad (2.5)$$

c. Effective local electric force:

$$\bar{E}_k = -\frac{\partial W}{\partial P_k} = -(a_{kj} P_j + f_{kl ij} \varepsilon_{ij,l}) \quad (2.6)$$

d. Polarization gradient force:

$$E_{ij} = \frac{\partial W}{\partial P_{j,i}} = b_{ijkl} P_{l,k} + e_{ijkl} \varepsilon_{kl} + b_{ij}^0 \quad (2.7)$$

We will concentrate in the isotropic response and in this case the material tensors become:

$$a_{ij} = a \delta_{ij} \quad (2.8)$$

$$c_{ijkl} = c_{12} \delta_{ij} \delta_{kl} + c_{44} (\delta_{ik} \delta_{jl} + \delta_{jk} \delta_{il}) \quad (2.9)$$

Table 1
Mutually exclusive boundary conditions for the flexoelectric problem.

Mutually Exclusive Boundary Conditions	
Essential (Dirichlet) Boundary Conditions	Dynamic (Neumann) Boundary Conditions
P_i Surface polarization	$n_j E_{ji}$ Higher order electric field
Φ Surface electric potential	$n_i (\epsilon_0 \ E_i\ - \ P_i\) = \sigma_s$ Surface charge
Du_i Displacement normal derivative	$r_i = \tau_{kji} n_k n_j$ Higher order traction
u_i Surface displacement	$t_i = \sigma_{ij} n_j - \tau_{kji,k} n_j + (D_j n_i) n_j n_k \tau_{kji} - D_j (\tau_{kji} n_k)$ Surface traction

n_i is the unit normal vector pointing outside the body.

$D \equiv n_k \partial / \partial x_k$ is the normal to the surface derivative.

$D_j \equiv (\delta_{jk} - n_j n_k) \partial / \partial x_k$ is the tangential to the surface derivative.

$\| \| = ()^+ - ()^-$ is the jump from outside of the body (+) to the inside of the body (-).

σ_s is the surface charge imposed on the dielectric boundary.

$$f_{ijkl} = f_{12} \delta_{ij} \delta_{kl} + f_{44} (\delta_{ik} \delta_{jl} + \delta_{jk} \delta_{il}) \tag{2.10}$$

$$e_{ijkl} = e_{12} \delta_{ij} \delta_{kl} + e_{44} (\delta_{ik} \delta_{jl} + \delta_{jk} \delta_{il}) \tag{2.11}$$

$$b_{ijkl} = b_{12} \delta_{ij} \delta_{kl} + b_{44} (\delta_{ik} \delta_{jl} + \delta_{jk} \delta_{il}) + b_{77} (\delta_{ik} \delta_{jl} - \delta_{jk} \delta_{il}) \tag{2.12}$$

$$b_{ij}^0 = b_0 \delta_{ij} \tag{2.13}$$

where δ_{ij} is Kronecker's delta (identity tensor). All material constants are positive definite and bounded. The dielectric susceptibility χ relates to the dielectric constant of vacuum ϵ_0 as $1/a = \chi \epsilon_0$. The classic elastic dielectric case is obtained, if $f_{ijkl} = 0$ and $e_{ijkl} = 0$, whereas the classic elastic case requires additionally $a_{ij} = 0$ and $b_{ij}^0 = 0$. If only $f_{ijkl} = 0$, we recover the formulation of Mindlin (1968; 1969) for a dielectric solid with polarization gradient. The effective flexocoupling tensor is $e_{ijkl} - f_{ijkl}$. The flexoelectric tensor is defined as $\mu_{ijkl} = a^{-1} f_{ijkl}$ [C/m], Sharma et al. (2010).

Using Hamilton's principle (least action), that is minimization of the total electric enthalpy with respect to u_i and P_i in the whole body volume V and arbitrary time interval $(0, t_1)$,

$$\int_0^{t_1} \int_V \delta(\bar{H} - T) dV dt = 0 \tag{2.14}$$

we obtain the Euler conditions for all the material points of the body (in the presence of body forces X_i [N/m³] and external electric field E_i^0 [N/C]): a. Conservation of linear momentum:

$$\sigma_{ji,j} - \tau_{kji,jk} + X_i = \rho \ddot{u}_i \tag{2.15}$$

b. Conservation of electric field (intramolecular forces):

$$\bar{E}_j + E_{ji,i} + E_j + E_j^0 = 0 \tag{2.16}$$

Note that in right hand side of Eq. (2.16) the polarization inertia $d_0 \ddot{\bar{P}}$ is considered to be negligible. c. Gauss' law (ρ^f density of charges) inside the body:

$$D_{,ii} = \epsilon_0 E_{,i,i} + P_{,i,i} = -\epsilon_0 \Phi_{,ii} + P_{,i,i} = \rho^f \tag{2.17}$$

where $D_i = \epsilon_0 E_i + P_i$ is the electric displacement. Outside the body, $\Phi_{,ii} = 0$. d. Maxwell-Faraday equations outside the body (in absence of magnetic flux):

$$\nabla \times \vec{E} = \vec{0} \tag{2.18}$$

where ∇ is the gradient operator, or, using the alternating Levi-Civita tensor, $\epsilon_{ijk} E_{k,j} = 0$. The corresponding, work conjugate, boundary conditions are summarized in Table 1. The electric boundary conditions can be materialized with appropriate steady state currents applied by surface conductors, Jackson (1975). In the present approach, the Maxwell stresses $D_j \bar{E}_i - (D_k \bar{E}_k) \delta_{ij} / 2$ are considered much smaller than the mechanical stresses σ_{ij} . In a similar manner we ignore the electrostatic stresses $-E_{kj} P_{k,i} + (E_{kl} P_{k,l}) \delta_{ij} / 2$. Such stresses

are negligible, if the dilatation strain is much smaller than the other strains. For a thorough discussion of the influence of Maxwell and electrostatic stresses in flexoelectricity refer to [Hu and Shen \(2010\)](#). The time derivative of the polarization gives rise to a magnetic field according to the Maxwell-Ampere law which has been discussed by [Giannakopoulos and Rosakis \(2022\)](#).

The initial conditions are

$$\begin{aligned} u_i(\vec{x}, 0) &= u_i^0(\vec{x}) \\ \dot{u}_i(\vec{x}, 0) &= \dot{u}_i^0(\vec{x}) \\ P_i(\vec{x}, 0) &= P_i^0(\vec{x}) \end{aligned} \quad (2.19)$$

where u_i^0 is the initial displacement vector, \dot{u}_i^0 is the initial velocity vector and P_i^0 is the initial polarization vector. The initial fields are considered to be known and are often taken to be zero.

Furthermore, assuming zero free electron density, zero body forces and zero initial electric field ($\rho^f = 0[C/m^3]$, $X_i = 0[N/m^3]$, $E_i^0 = 0[N/C]$), we transform [Eqs. \(2.15\)](#) and [\(2.16\)](#) into Navier-type of equations:

$$c_{44}\nabla^2 u_i + (c_{12} + c_{44})\nabla_i(\nabla_k u_k) + (e_{44} - f_{12})\nabla^2 P_i + (e_{12} + e_{44} - 2f_{44})\nabla_i(\nabla_k P_k) = \rho \ddot{u}_i \quad (2.20)$$

$$\begin{aligned} (e_{44} - f_{12})\nabla^2 u_i + (e_{12} + e_{44} - 2f_{44})\nabla_i(\nabla_k u_k) + (b_{44} + b_{77})\nabla^2 P_i + (b_{12} + b_{44} - b_{77})\nabla_i(\nabla_k P_k) \\ - aP_i + E_i = 0 \end{aligned} \quad (2.21)$$

where, $\nabla^2 = \nabla_k \nabla_k = \partial^2/\partial x_1^2 + \partial^2/\partial x_2^2 + \partial^2/\partial x_3^2$ is the Laplacian operator, $\nabla^4 = \nabla^2 \nabla^2$ is the biharmonic operator. Note that, if $f_{ijkl} = 0$, $e_{ijkl} = 0$ and $a_{ij} = 0$, we obtain from (2.20) the classic elastodynamic equations and (2.21) is identically zero.

Starting from the Navier-type of [Eqs. \(2.21\)](#), we take the gradient on (2.21) and on (2.17) and eliminate the electric field to obtain:

$$\begin{aligned} (e_{44} - f_{12})\nabla \cdot \nabla^2 \vec{u} + (e_{12} + e_{44} - 2f_{44})\nabla^2 \nabla \cdot \vec{u} \\ + (b_{44} + b_{77})\nabla \cdot \nabla^2 \vec{P} + (b_{12} + b_{44} - b_{77})\nabla^2 \nabla \cdot \vec{P} - (a + \epsilon_0^{-1})\nabla^2 \nabla \cdot \vec{P} = 0 \end{aligned} \quad (2.22)$$

Thus the reformulation of the problem leads to solving two coupled [Eqs. \(2.20\)](#) and [\(2.22\)](#) with respect to the displacement vector u_i and the polarization vector P_i .

To clarify the new statement of the problem, we will follow the approach of [Giannakopoulos and Rosakis \(2020\)](#) and decouple the problem to one that involves only the displacement vector (dynamic equation) and another that involves the polarization vector in relation to the displacement (transfer equation). The representation of the general solution of (2.20), (2.22) has been given by [Giannakopoulos and Rosakis \(2020\)](#) as a Helmholtz decomposition of both the displacement and the polarization vectors as

$$\vec{u} = \nabla \phi + \nabla \times \vec{H}^* \nabla \cdot \vec{H}^* = 0 \quad (2.23)$$

$$\vec{P} = \nabla \chi^* + \nabla \times \vec{K} \nabla \cdot \vec{K} = 0 \quad (2.24)$$

where $\phi(\vec{x}, t)$ and $\chi^*(\vec{x}, t)$ are scalar functions, whereas $\vec{H}^*(\vec{x}, t)$ and $\vec{K}(\vec{x}, t)$ are vector functions that are solutions of

$$\nabla^2 \phi - \ell_p^2 \nabla^4 \phi = \frac{1}{c_p^2} \left(\ddot{\phi} - h_p^2 \nabla^2 \ddot{\phi} \right) \quad (2.25)$$

$$\nabla^2 \vec{H}^* - \ell_s^2 \nabla^4 \vec{H}^* = \frac{1}{c_s^2} \left(\ddot{\vec{H}}^* - h_s^2 \nabla^2 \ddot{\vec{H}}^* \right) \quad (2.26)$$

$$\nabla^2 \chi^* - \ell_p^2 \nabla^4 \chi^* = \frac{1}{c_p^2} \left(\frac{e_{11} - f_{11}}{a + \epsilon_0^{-1}} \nabla^2 \ddot{\phi} \right) \quad (2.27)$$

$$\nabla^2 \vec{K} - \ell_s^2 \nabla^4 \vec{K} = \frac{1}{c_s^2} \left(\frac{e_{44} - f_{12}}{a} \nabla^2 \ddot{\vec{H}}^* \right) \quad (2.28)$$

where the characteristic dilatation and shear speeds appear as in classic elastodynamics

$$c_p = \sqrt{\frac{c_{11}}{\rho}} = \sqrt{\frac{c_{12} + 2c_{44}}{\rho}} = \sqrt{\frac{\lambda + 2\mu}{\rho}} = \sqrt{\frac{E(1-\nu)}{\rho(1+\nu)(1-2\nu)}} \quad (2.29)$$

$$c_s = \sqrt{\frac{c_{44}}{\rho}} = \sqrt{\frac{\mu}{\rho}} = \sqrt{\frac{E}{2\rho(1+\nu)}} < c_p$$

Table 2
Typical material constants.

Constant	Units	NaI 110 K [100]	KI 95 K [100]	NaCl 80 K [100]	KCl 80 K [100]	PMMA 300 K
$\mu = c_{44}$	GPa	7.2	4.4	12.8	6.8	2.215
$\lambda + 2\mu = c_{12} + 2c_{44}$	GPa	21.4	12.7	38.4	19.9	9.585
$/e_{44}f_{12} /$	Nm/C = V	-0.210	-0.194	-0.242	-0.215	7.015
$/e_{11}f_{11} /$	Nm/C = V	0.381	0.342	0.467	0.392	56.12
b_{11}	Nm ⁴ /C ²	0.712 10 ⁻⁹	1.110 10 ⁻⁹	0.688 10 ⁻⁹	1.20 10 ⁻⁹	1.807 10 ⁻⁶
$(b_{44} + b_{77})$	Nm ⁴ /C ²	0.712 10 ⁻⁹	1.110 10 ⁻⁹	0.688 10 ⁻⁹	1.20 10 ⁻⁹	1.807 10 ⁻⁶
a	Nm ² /C ²	137 10 ⁸	176 10 ⁸	174 10 ⁸	243 10 ⁸	6.275 10 ¹⁰
ρ	kg/m ³	3670	3120	2160	1980	1180
c_s	m/s	1401	1188	2434	1853	1370
c_p	m/s	2415	1994	4216	3170	2850
ℓ_p	nm	0.07500	0.9184	0.07236	0.09322	2.9
h_p	nm	0.07498	0.09221	0.07265	0.09351	3.2075
ℓ_s	nm	0.2270	0.2501	0.1981	0.2216	4.521
h_s	nm	0.2280	0.2511	0.1988	0.2222	4.535
a_0	nm	0.323	0.353	0.281	0.314	
Lattice length						
Ω_p	THz	33	43	50	40	
Ω_s	THz	22	32	31	27	
$-b^0$	Nm/C	1.26 10 ⁻²	1.15 10 ⁻²	1.44 10 ⁻²	1.29 10 ⁻²	

$\epsilon_0 = 1/(36\pi) \times 10^{-9} \approx 8.854 \times 10^{-12} \text{ C}^2 \text{ N}^{-1} \text{ m}^{-2}$ (F/m) dielectric constant at vacuum.

where E , and ν are the Young's modulus and the Poisson's ratio respectively, and (λ, μ) are the classic Lamé constants. Moreover, in the above equations four lengths appear, defined by

$$\{\mu, a, f_{12}, f_{44}, e_{44}, b_{44} + b_{77}, \mu(b_{44} + b_{77}) - e_{44}^2\} > 0$$

$$\ell_s^2 = \frac{(b_{44} + b_{77})}{a} - \frac{(e_{44} - f_{12})^2}{\mu a} \geq 0 \tag{2.30}$$

$$h_s^2 = \frac{(b_{44} + b_{77})}{a} \geq \ell_s^2 \geq 0$$

$$\{b_{11} = b_{12} + 2b_{44}, a, f_{11} = f_{12} + 2f_{44}, e_{11} = e_{12} + 2e_{44}, f_{44}, (\lambda + 2\mu)b_{11} - e_{11}^2\} > 0$$

$$\ell_p^2 = \frac{b_{11}}{a + \epsilon_0^{-1}} - \frac{(e_{11} - f_{11})^2}{(\lambda + 2\mu)(a + \epsilon_0^{-1})} \geq 0 \tag{2.31}$$

$$h_p^2 = \frac{b_{11}}{a + \epsilon_0^{-1}} \geq \ell_p^2 \geq 0$$

Thus, we obtain two “micro-structural” related lengths (ℓ_p, ℓ_s) and two “micro-inertial” related lengths (h_p, h_s). Similar ‘micro-structural’ lengths to (ℓ_p, ℓ_s) have been shown by [Sharma et al. \(2007\)](#), however, the ‘micro-inertial’ lengths (h_p, h_s) have been introduced by [Giannakopoulos and Rosakis \(2020\)](#) for the case of dynamics. Note that the positiveness of the lengths stems from the assumed convexity (and positive definiteness) of the energy density. They give exactly the flexoelectric coefficient bounds suggested by [Yudin et al. \(2014\)](#). Gradient dielectricity also yields the internal lengths (ℓ_p, ℓ_s) and (h_p, h_s) while, flexo-electricity leads to higher microstructural lengths, compared to gradient dielectricity. The mechanical response is similar to that of the Mindlin’s model of linear elastic solids with microstructure ([Mindlin, 1963](#)). We further note that polarization exhibits a size effect similar to the size effect of the mechanical displacement.

Typical material constants for PMMA (poly-methyl-methacrylate) were estimated and are shown in [Table 2](#) and are obtained from [Giannakopoulos and Rosakis \(2020\)](#). A rather complete material data for alkali halides have been found by [Askar et al. \(1970\)](#) and are also summarized in [Table 2](#). The data for NaCl and KCl confirm the neutron scattering dispersion relations of [Raunio et al. \(1969\)](#) and [Raunio and Alqvist \(1969\)](#), in excellent accord with the atomistic calculations of [Maranganti and Sharma \(2009\)](#).

The general solution starts from the mechanical response, solving (2.25) for $\phi(\vec{x}, t)$, and (2.26) for $\vec{H}^*(\vec{x}, t)$. Once the displacement vector is found, the polarization vector can be found from the solution of (2.27) for $\chi^*(\vec{x}, t)$ and (2.28) for $\vec{K}(\vec{x}, t)$.

3. The dispersion relations

The discrete atomic structure of crystals implies a dispersive medium, even in the absence of the flexoelectric effect (Brillouin, 1946). In the present case, the relation between the frequency $\omega/2\pi$ and the wave number k can be obtained from the dynamic equilibrium Eqs. (2.25) for the dilatational waves, and (2.26) for the shear waves. Due to conservation of energy assumed in the present model, the frequency is real, whereas the wave number may be complex. The dynamic equation will provide two types of dispersion relations: mechanical and optical. For the time we will assume that k is real (traveling waves).

3.1. Mechanical modes

The mechanical modes are controlled by Eqs. (2.25) and (2.26). Separation of variables (see Appendix A) leads to a solution of the type $\phi = \bar{\phi} \exp[-i\omega t] \exp[ik(\bar{n} \cdot \bar{x})]$, where \bar{n} is the in-plane unit direction vector of travelling waves and $i = \sqrt{-1}$. Replacing this type of solution in (2.25), we obtain a dispersion relation for the dilatation mechanical wave as:

$$\omega^2 = k^2 c_p^2 \frac{1 + \ell_p^2 k^2}{1 + h_p^2 k^2} \quad (3.1)$$

and the phase velocity reads as:

$$\left(\frac{\omega}{k}\right)_p = c_p \left(\frac{1 + \ell_p^2 k^2}{1 + h_p^2 k^2}\right)^{1/2} \leq c_p \quad (3.2)$$

The dilatational energy propagates with group velocity $d\omega/dk$ which reads as:

$$\begin{aligned} \left(\frac{d\omega}{dk}\right)_p &= \left(\frac{\omega}{k}\right)_p + c_p (\ell_p^2 k^2 - h_p^2 k^2) (1 + \ell_p^2 k^2)^{-1/2} (1 + h_p^2 k^2)^{-3/2} = \\ \left(\frac{\omega}{k}\right)_p \frac{1 + k^2 \ell_p^2}{1 + k^2 h_p^2} &= \left(\frac{\omega}{k}\right)_p^3 \frac{1}{c_p^2} \leq \left(\frac{\omega}{k}\right)_p \end{aligned} \quad (3.3)$$

So the group velocity is less than the phase velocity, because $h_p^2 \geq \ell_p^2$, and varies smoothly between the values:

$$k \rightarrow 0, \quad \left(\frac{d\omega}{dk}\right)_p = \left(\frac{\omega}{k}\right)_p = c_p \quad (3.4)$$

$$k \rightarrow \infty, \quad \left(\frac{d\omega}{dk}\right)_p = c_p \frac{\ell_p^2}{h_p^2} \leq c_p \quad (3.5)$$

Note that for $h_p = \ell_p$ or $(h_p, \ell_p) \rightarrow 0$, the dilatational wave velocity degenerates into the non-dispersive velocity of classical elastodynamics.

Assuming now a solution of the type $\vec{H} = \vec{H} \exp[-i\omega t] \exp[ik(\bar{n} \cdot \bar{x})]$, where \bar{n} is the in-plane unit direction vector of travelling waves, and replacing this type of solution in (2.26), we obtain a dispersion relation for the shear mechanical wave as:

$$\omega^2 = k^2 c_s^2 \frac{1 + \ell_s^2 k^2}{1 + h_s^2 k^2} \quad (3.6)$$

and the phase velocity reads as:

$$\left(\frac{\omega}{k}\right)_s = c_s \left(\frac{1 + \ell_s^2 k^2}{1 + h_s^2 k^2}\right)^{1/2} \quad (3.7)$$

The dilatational energy propagates with group velocity which reads as:

$$\begin{aligned} \left(\frac{d\omega}{dk}\right)_s &= \left(\frac{\omega}{k}\right)_s + c_s (\ell_s^2 k^2 - h_s^2 k^2) (1 + \ell_s^2 k^2)^{-1/2} (1 + h_s^2 k^2)^{-3/2} = \\ \left(\frac{\omega}{k}\right)_s \frac{1 + k^2 \ell_s^2}{1 + k^2 h_s^2} &= \left(\frac{\omega}{k}\right)_s^3 \frac{1}{c_s^2} \leq \left(\frac{\omega}{k}\right)_s \end{aligned} \quad (3.8)$$

For real wave number k , the group velocity is in the same direction with the phase velocity. Note that for $h_s = \ell_s$ or $(h_s, \ell_s) \rightarrow 0$, the shear wave velocity degenerates into the non-dispersive velocity of classical elastodynamics. As for the dilatational waves, the group velocity for the shear waves is less than their phase velocity and varies smoothly between the values:

$$k \rightarrow 0, \left(\frac{d\omega}{dk} \right)_s = \left(\frac{\omega}{k} \right)_s = c_s \tag{3.9}$$

$$k \rightarrow \infty, \left(\frac{d\omega}{dk} \right)_s = c_s \frac{\ell_s^2}{h_s^2} \leq c_s \tag{3.10}$$

Dispersion is due to the ratio of the micro-structural to the micro-inertial lengths. If these ratios are one, we return to the classic non-dispersive case. Our analysis predicts that the micro-inertia lengths have an important effect at high frequencies with wave lengths that are comparable with the micro-structural length. Comparing the phase velocities, we observe that

$$\left(\frac{c_p}{c_s} \right)^2 \geq \frac{b_{44} + b_{77}}{b_{11}} \Leftrightarrow \left(\frac{\omega}{k} \right)_p \geq \left(\frac{\omega}{k} \right)_s \text{ and } \left(\frac{d\omega}{dk} \right)_p \geq \left(\frac{d\omega}{dk} \right)_s \tag{3.11}$$

Indeed, the known material parameters indicated that the ratio $(b_{44} + b_{77})/b_{11}$ is never larger than 2 and c_p^2/c_s^2 is not smaller than 2 (see for example Table 2). Nevertheless, condition (3.11) does not stem from any theory and should not be taken for granted for all natural and synthetic dielectric materials. Condition (3.11) is also necessary and sufficient for a similar inequality for the group velocity.

3.2. Polarization modes

The polarization modes are controlled by Eqs. (2.27) and (2.28) which indicate strong coupling with the mechanical modes given by eqs. (2.25) and (2.26). Therefore, from separation of variables $\phi = \bar{\phi} \exp[-i\omega t] \exp[ik(\vec{n} \cdot \vec{x})]$, and so necessarily $\chi^* = S_p \bar{\phi} \exp[-i\omega t] \exp[ik(\vec{n} \cdot \vec{x})]$. Consequently, the transfer Eq. (2.27) provides a “dispersion-like” relation which we will accept as a soft-mode optical dispersion related to the dilatational mechanical waves

$$\omega^2 = c_p^2 \frac{-(a + \epsilon_0^{-1})}{e_{11} - f_{11}} S_p [1 + \ell_p^2 k^2] \tag{3.12}$$

For real frequencies, we must have $-(a + \epsilon_0^{-1})S_p/(e_{11} - f_{11}) > 0$ and the two fields must be in phase. Interestingly, Huller (1969), using lattice dynamics and the quantum result of Barrett (1952) provides a soft-mode optical dispersion relation for perovskites of the type:

$$\omega^2 \approx \Omega_p^2 + \Lambda_p k^2 \tag{3.13}$$

In (3.13), Ω_p is a frequency at zero wave number (cut-off frequency) that is inversely proportional to the dielectric constant (or proportional to a in our presentation). This cut-off frequency can be estimated by Ginzburg’s formula $\Omega_p^2 = (a + \epsilon_0^{-1})ne^2/m$ where m is the effective mass of the ions, n is the number of ions per unit volume and e is the effective charge of the ions in the dielectric, Sannikov (1962). Eq. (3.12) does not hold if $\ell_p \approx h_p$, because in this case $e_{11} - f_{11} \approx 0$.

Comparing (3.12) and (3.13) we can identify Huller’s parameters as

$$\Omega_p^2 = \frac{-(a + \epsilon_0^{-1})}{e_{11} - f_{11}} S_p c_p^2 \tag{3.14}$$

$$\Lambda_p = \Omega_p^2 \ell_p^2 \tag{3.15}$$

Next, assuming $\bar{H}^* = \bar{H} \exp[-i\omega t] \exp[ik(\vec{n} \cdot \vec{x})]$ and $\bar{K} = S_s \bar{K} \exp[-i\omega t] \exp[ik(\vec{n} \cdot \vec{x})]$, the transfer Eq. (2.28) provides a “dispersion-like” relation which we will accept as a soft-mode optical dispersion related to the shear mechanical waves

$$\omega^2 = c_s^2 \frac{-a}{e_{44} - f_{44}} S_s [1 + \ell_s^2 k^2] \tag{3.16}$$

For real frequencies, we must have $-aS_s/(e_{44} - f_{44}) > 0$ and the two field must be in-phase. Following Huller (1969), the soft-mode optical dispersion relation related to shear type of mechanical waves is of the form:

$$\omega^2 \approx \Omega_s^2 + \Lambda_s k^2 \tag{3.17}$$

In (3.17), Ω_s is a frequency at zero wave number that is inversely proportional to the dielectric constant (or proportional to a in our presentation). The dielectric constant depends critically on the temperature, Barrett (1952). Comparing (3.16) and (3.17) we can identify Huller’s parameters as

$$\Omega_s^2 = \frac{-a}{e_{44} - f_{44}} S_s c_s^2 \tag{3.18}$$

$$\Lambda_s = \Omega_s^2 \ell_s^2 \tag{3.19}$$

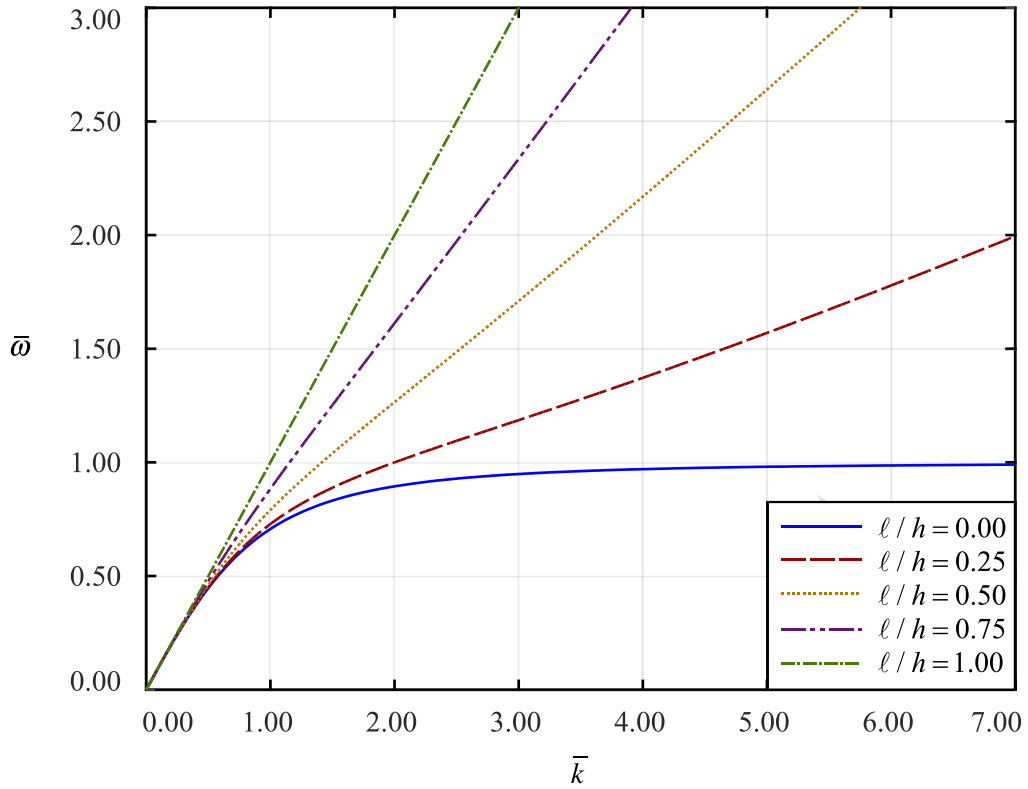


Fig. 1a. Normalized plot of the mechanical modes, implied by Eqs. (3.1) and (3.6). The normalized frequency is $\bar{\omega} = \omega h_{p,s} / c_{p,s}$ and the normalized wave number is $\bar{k} = k h_{p,s}$. The suffix p and s denote dilatational and shear part respectively.

Values of Ω_p, Ω_s can be found in several books, e.g. Kittel (1971). Eq. (3.12) does not hold if $\ell_s \approx h_s$, because in this case $e_{44} - f_{44} \approx 0$.

It is interesting to note that in case $\Lambda_{p,s} \approx 0$ (semiconductors), the maximum frequencies take the general form (disregard indices p and s for shortness)

$$\max \omega \approx \frac{c}{h} \tag{3.20}$$

for the mechanical response and

$$\omega^2 \approx \Omega^2 \tag{3.21}$$

for the optical branch of the dispersion relation.

Fig. 1a shows the normalized plot of the mechanical modes, implied by Eqs. (3.1) and (3.6). Fig. 1b shows the normalized plot of the optical modes, implied by Eqs. (3.12) and (3.14). The normalized wave number is $\bar{k} = k h_{p,s}$. The suffix p,s denotes dilatational and shear part accordingly. The normalized frequency for the mechanical modes is $\bar{\omega} = \omega h_{p,s} / c_{p,s}$. The normalized frequency for the optical modes is $\bar{\omega} = \omega / \Omega_{p,s}$.

The normalized dispersion equations take the form

$$\bar{\omega} = \bar{k} \left(\frac{1 + (\ell_{p,s} / h_{p,s})^2 \bar{k}^2}{1 + \bar{k}^2} \right)^{1/2} \tag{3.22}$$

for the mechanical modes and

$$\bar{\omega} = \left[1 + (\ell_{p,s} / h_{p,s})^2 \bar{k}^2 \right]^{1/2} \tag{3.23}$$

for the optical modes. Fig. 2a shows the normalized mechanical phase velocities $\bar{\omega} / \bar{k}$, as a function of the normalized wave number \bar{k} . Then, from (3.2) and (3.7), we obtain:

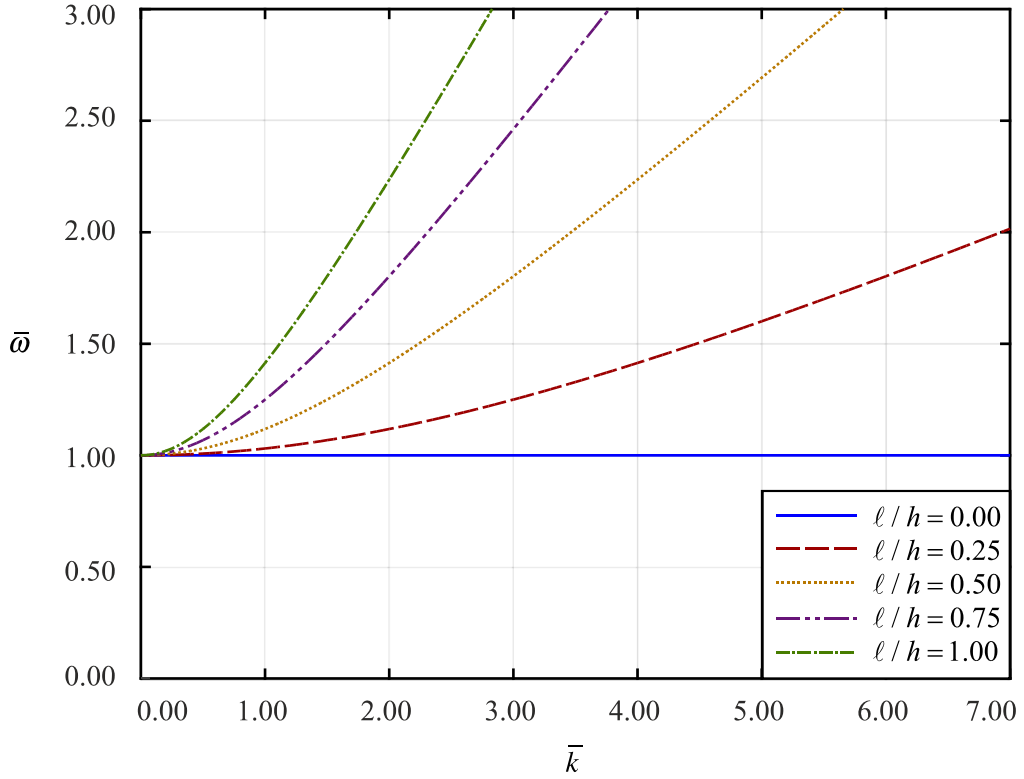


Fig. 1b. Normalized plot of the optical modes, implied by Eqs. (3.12) and (3.14). The normalized frequency is $\bar{\omega} = \omega/\Omega_{p,s}$ and the normalized wave number is $\bar{k} = kh_{p,s}$. The suffix p and s denote dilatational and shear part respectively.

$$\frac{\bar{\omega}}{\bar{k}} = \left(\frac{1 + (\ell_{p,s}/h_{p,s})^2 \bar{k}^2}{1 + \bar{k}^2} \right)^{1/2} \quad (3.24)$$

Fig. 2b shows the normalized optical phase velocity $\bar{\omega}/\bar{k}$, as a function of the normalized wave number \bar{k} . Then, from (3.23), we obtain:

$$\frac{\bar{\omega}}{\bar{k}} = \frac{1}{\bar{k}} \left[1 + (\ell_{p,s}/h_{p,s})^2 \bar{k}^2 \right]^{1/2} \quad (3.25)$$

Fig. 3a shows the normalized mechanical group velocities $d\bar{\omega}/d\bar{k}$, as a function of the normalized wave number \bar{k} . Then, from (3.3) and (3.8), we obtain:

$$\frac{d\bar{\omega}}{d\bar{k}} = \frac{\bar{\omega}}{\bar{k}} + \left((\ell_{p,s}/h_{p,s})^2 \bar{k}^2 - \bar{k}^2 \right) \left(1 + (\ell_{p,s}/h_{p,s})^2 \bar{k}^2 \right)^{-1/2} (1 + \bar{k}^2)^{-3/2} \quad (3.26)$$

In the Appendix B we show that the mechanical group velocities (3.26) are the velocities of the transfer of the time average of the power per unit area to the twice the time average of the kinetic energy across the plane of a time-harmonic plane wave (longitudinal and transverse) that travel inside the body. In Appendix C we start from the conservation of wave crests and show that the wave lengths propagate with the group velocity and provide an alternative formula to calculate the group velocity.

Fig. 3b shows the normalized optical group velocities $d\bar{\omega}/d\bar{k}$, as a function of the normalized wave number \bar{k} . Then, from (3.23), we obtain:

$$\frac{d\bar{\omega}}{d\bar{k}} = (\ell_{p,s}/h_{p,s})^2 \bar{k} \left(1 + (\ell_{p,s}/h_{p,s})^2 \bar{k}^2 \right)^{-1/2} \quad (3.27)$$

In these figures, there is a free parameter in the range $0 \leq \ell_{p,s}/h_{p,s} \leq 1$. As this parameter increases from 0 to 1, the mechanical dispersion relations start with the same slope at low frequencies and attain a linear asymptote at high frequencies, proportional to $\ell_{p,s}/h_{p,s}$. The optical dispersion relationships start at a high initial frequency and also attain a linear asymptote at high frequencies, proportional to $\ell_{p,s}/h_{p,s}$. Note that the optical frequencies are greater than the mechanical frequencies. The normalized phase and group velocities approach the value $\ell_{p,s}/h_{p,s}$ at high wave numbers $\bar{k} \rightarrow \infty$. The phase velocities are greater than the group velocities. The mechanical phase velocity, the mechanical group velocity and the optical group velocities have an upper bound of 1. The optical phase

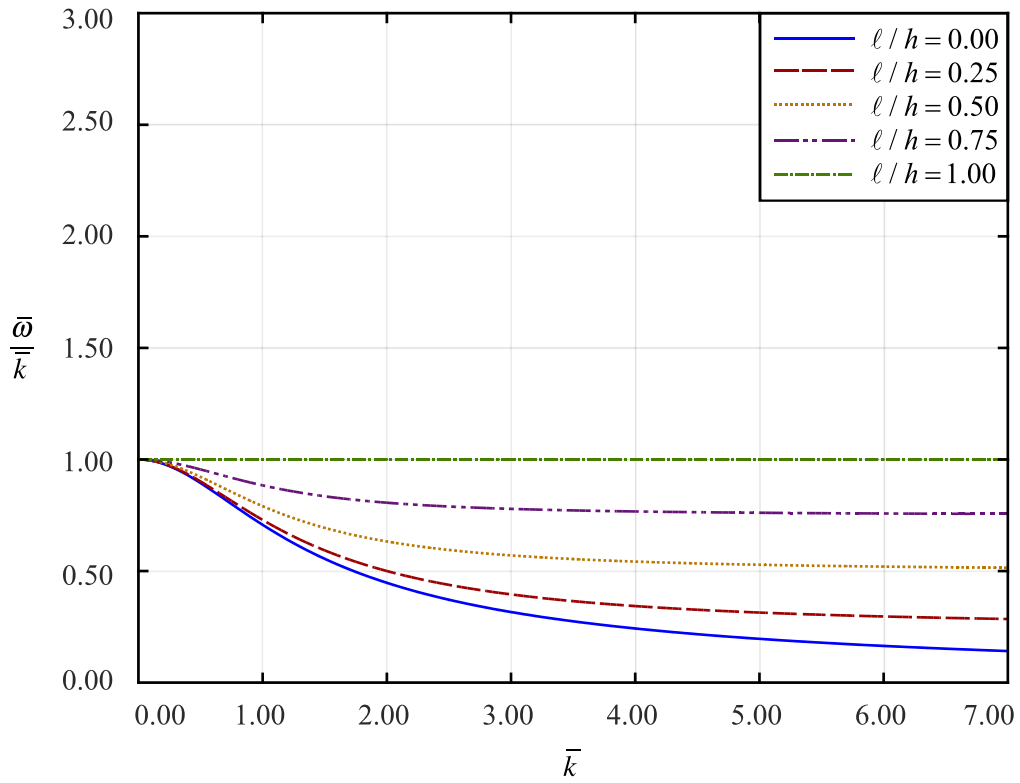


Fig. 2a. Normalized mechanical phase velocity $\bar{\omega}/\bar{k}$, as a function of the normalized wave number \bar{k} . The normalization is as in Fig. 1.

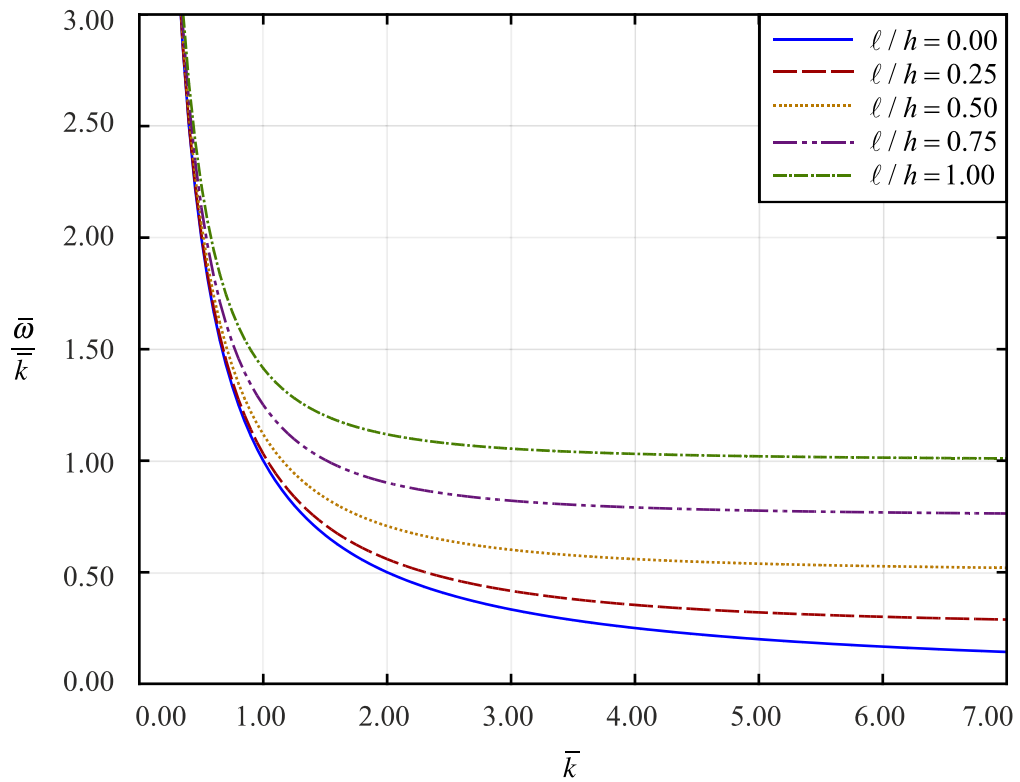


Fig. 2b. Normalized optical phase velocity $\bar{\omega}/\bar{k}$, as a function of the normalized wave number \bar{k} . The normalization is as in Fig. 1.

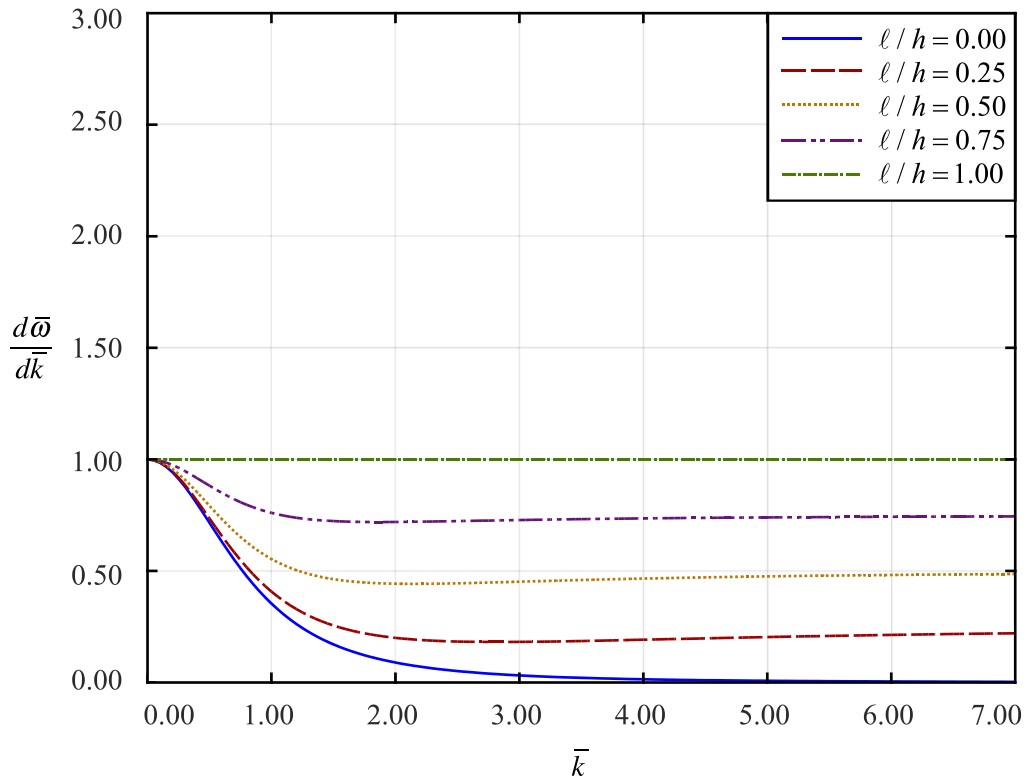


Fig. 3a. Normalized mechanical group velocity $d\bar{\omega}/d\bar{k}$, as a function of the normalized wave number \bar{k} . The normalization is as in Fig. 1.

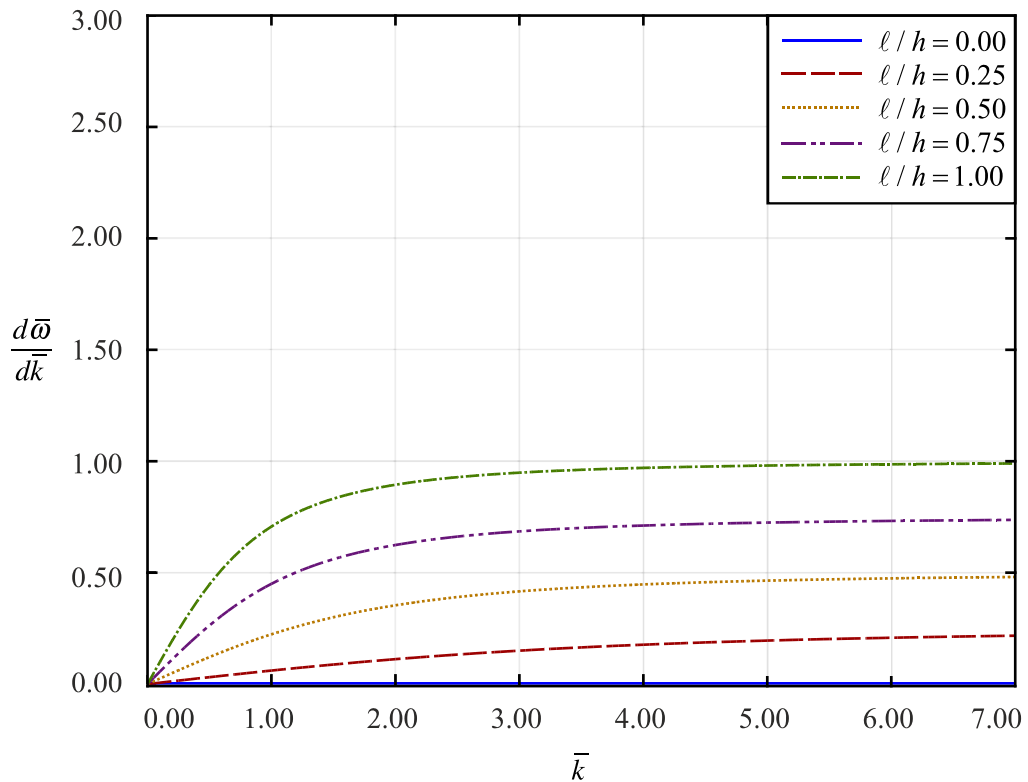


Fig. 3b. Normalized optical group velocity $d\bar{\omega}/d\bar{k}$, as a function of the normalized wave number \bar{k} .

velocities are unbounded for small wave numbers $\bar{k} \rightarrow 0$. Note that the dilatation group velocity is greater than the shear group velocity for both the mechanical and the optical modes.

The derived dispersion relation (3.20) can be also related to the bond charge model of Weber (1974) that includes metal-like bonding by central forces between nearest-neighbor ions and covalent binding in interactions involving the bond actions, observed in many semiconducting material.

$$\frac{a_0^2}{4} \omega^2 = c^2 \frac{\sin^2(ka_0/2)}{1 + 2(f'/f)\sin^2(ka_0/2)} \tag{3.28}$$

where a_0 is the atomic cell dimension, and f'/f is the ratio of the ionic forces to the bond charge forces. The result holds for the Brillouin zone $0 \leq ka_0/2 \leq \pi/2$. For wave numbers less than $1/a_0$, the ratio of the internal lengths of the present theory indicates that the micro-structural length relates to the atomic cell dimension $a_0/2 = \ell$. The ratio of the ionic forces to the bond charge forces ($f'/f \gg 1$) can give an estimate of the ratio of the micro-inertial length to the micro-inertial length,

$$h = \frac{a_0}{2} \left(1 + 2\frac{f'}{f}\right)^{1/2} \tag{3.29}$$

It is of interest to point that the dispersion relation of the type (3.22) approximates the dispersion of the fundamental mode of a circular cylinder of radius R acting as a wave guide of longitudinal waves (Pochhammer frequency equation), Achenbach (1990). In this case, an analogy can be established by assuming a micro-structural length and a micro-inertia length as

$$\ell^2 \rightarrow \frac{\nu R}{2} \tag{3.30}$$

$$\frac{h^2}{\ell^2} \rightarrow \frac{0.862 + 1.14\nu}{1 + \nu} \sqrt{2(1 + \nu)} > 1$$

with a characteristic wave velocity

$$c \rightarrow \sqrt{\frac{E}{\rho}} \tag{3.31}$$

In classic elasticity, plane strain waves in an elastic layer of thickness $2H$ give the Rayleigh-Lamb dispersion relations, Achenbach (1990). For real wave numbers, the longitudinal symmetric mode result resembles our dispersion relation (3.1), assuming $\ell^2/h^2 = (1 - \nu)^{1/2} \leq 1$. Another interesting analogy of the optical dispersion relation of the type (3.23) exist with the classic waveguides is the horizontally polarized shear waves propagating in an elastic layer of thickness $2H$ and is the first antisymmetric mode, Achenbach (1990). In this case, an analogy can be established by assuming a micro-structural length as

$$\ell^2 \rightarrow \frac{2H}{\pi} \tag{3.32}$$

$$\frac{h^2}{\ell^2} \rightarrow 0$$

with a characteristic wave velocity

$$c_s = \sqrt{\frac{E}{2(1 + \nu)\rho}} \tag{3.33}$$

and a cut-off frequency

$$\Omega_s \rightarrow \frac{\pi c_s}{2H} \tag{3.34}$$

4. Attenuation of the mechanical waves

Regarding the mechanical waves, solving (3.2) and (3.6) to express the wave number k as a function of the frequency $k(\omega)$, we obtain:

$$k_1^2(\omega) = \frac{2\omega^2}{c^2 - h^2\omega^2 + \sqrt{(c^2 - h^2\omega^2)^2 + 4\ell^2\omega^2c^2}} \geq 0 \tag{4.1}$$

and

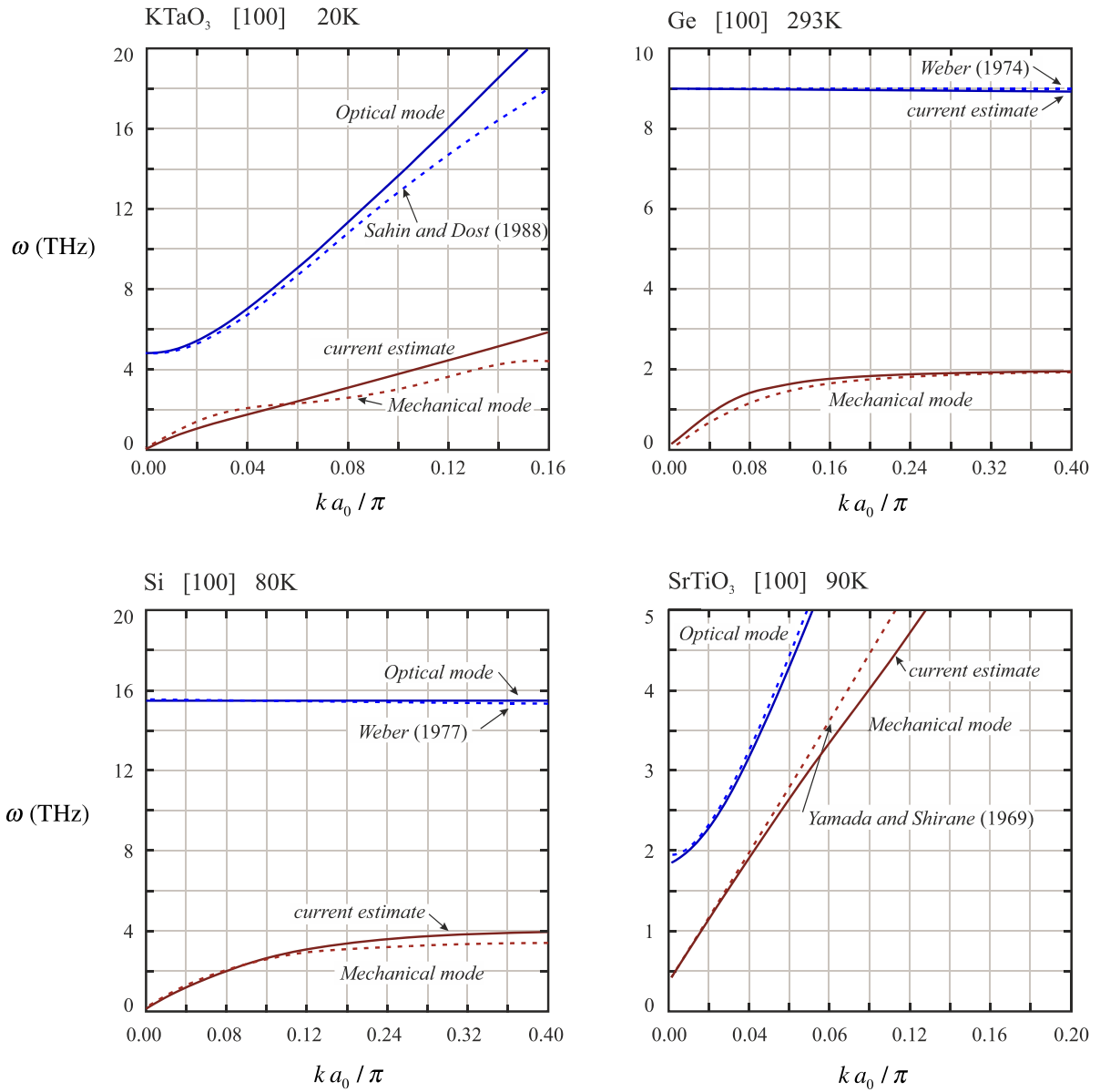


Fig. 4. The shear dispersion relations for (a) KTaO₃ (potassium tantalite, perovskite structure), (b) Ge (germanium, diamond structure), (c) Si (silicon, diamond structure) and (d) SrTiO₃ (strontium titanate, perovskite structure). The plots show the frequency ω versus the normalized wave number $0 \leq ka_0/\pi \leq 1$. The experimental results are: for Si from [Weber \(1977\)](#), for SrTiO₃ from [Yamada and Shirane \(1969\)](#), for KTaO₃ from [Sahin and Dost \(1988\)](#), and for Ge from [Weber \(1977\)](#). [Giannakopoulos and Zisis \(2020, 2021\)](#).

$$k_2^2(\omega) = \frac{2\omega^2}{c^2 - h^2\omega^2 - \sqrt{(c^2 - h^2\omega^2)^2 + 4\ell^2\omega^2c^2}} < 0 \quad (4.2)$$

In the above results we have $\{c = c_p, \ell = \ell_p \neq 0, h = h_p\}$ for the dilatational waves and $\{c = c_s, \ell = \ell_s \neq 0, h = h_s\}$ for the transverse waves. These results imply that the k_1 's are always real (associated to propagating or traveling waves) and the k_2 's are always imaginary (associated with standing or evanescent waves). Note that $1/h < |k_1| < 1/\ell, |k_2| > |k_1|$. The imaginary wave numbers imply attenuated or evanescent waves (with zero cut-off frequency) that do not exist in classical elasto-dynamics $\{\ell = 0, h = 0, k_1^2 = \omega^2/c^2\}$. This indicates that, depending on the initial and boundary conditions will lead to spatial attenuation of the mechanical waves due to the radiation of the electromagnetic waves that accompany the mechanical waves. Interestingly, classical elasto-dynamic dispersion relations can be obtained also for $\{\ell = h, k_1^2 = \omega^2/c^2\}$. The standing waves play a significant role in cases of reflexion and transmission at material discontinuity surfaces. Indeed, such evanescent waves have been shown at a biomaterial surface in the context of second gradient elastic continua ([dell'Isola et al., 2012](#)) and at the free surface of anti-plane couple stress materials ([Nobili et al., 2019](#)).

Table 3

Typical material constants calculated from the experimental dispersion curves of Fig. 4 (transverse mechanical and optical waves).

Property	SrTiO ₃ [100] 90 K	KTaO ₃ [100] 20 K	Ge [100] 293 K	Si [100] 80 K
a_0 (nm) known	0.391	0.399	0.566	0.543
ρ (kg/m ³) known	5174	6970	5360	2330
$c_{44} = \mu$ (GPa) fitted	122	107	40	79.1
α (10 ⁸ Nm ² /C ²) known	0.865	0.355	75.3	103
$(b_{44} + b_{77})$ (10 ⁻⁹ Nm ⁴ /C ²) Fitted	0.815	0.435	23.6	22.0
$(e_{44} - f_{12})$ (Nm/C = V) Fitted	- 1.9	6.00	(+/-) 8.80	- 11.0
Ω_s (THz) known	1.46	4.79	9.00	15.5
c_s (m/s) fitted	4856	3910	2732	5827
h_s (nm) fitted	0.93	3.50	1.37	1.46
ℓ_s (nm) fitted	0.72	1.66	1.31	1.41
$\min\gamma$ (10 ⁻¹⁷ kgm ³ /C ²)	0.40	0.15	0.93	0.43
$\max/M/$ (10 ⁻⁸ Vs ² /m ²)	14	10	18	10

In the above result we have $\{c = c_p, h = h_p\}$ for the dilatational waves and $\{c = c_s, h = h_s\}$ for the transverse waves. Let us select the imaginary wave number $k_2 = i|k_2|$. Then the dispersion relation becomes

$$\omega^2 = c^2 |k_2|^2 \left(\frac{-1 + \ell^2 |k_2|^2}{1 - h^2 |k_2|^2} \right) \quad (4.3)$$

The frequency is real, so $1/h < |k_2| \leq 1/\ell$ with $\omega = 0$ for $|k_2| = 1/\ell$ and $\omega \rightarrow +\infty$ for $|k_2| \rightarrow 1/h$. The imaginary wave numbers imply attenuated or evanescent waves which now depend on frequency and on the micro-inertial length h .

5. Comparison with experimental results

The dispersion relations obtained by the present analysis can provide a good approximation to many experimental dispersion curves of flexoelectric materials for a moderate Brillouin region $0 \leq ka_0/\pi < 0.2$. Examples of the shear type dispersion relations are shown in Fig. 4 Giannakopoulos and Zisis (2020, 2021), where we show the experimental dispersion relations for (a) KTaO₃, (b) Ge, (c) Si and (d) SrTiO₃. The experimental dispersion curves concern particular temperatures and were obtained from the neutron scattering method. The experimental dispersion relations can be utilized to obtain certain material properties by fitting our analytic results to both the acoustical modes and the optical modes. In case of known material properties the fitting should be direct. The dispersion plots show the frequency ω versus the normalized wave number ka_0/π . The experimental results have been obtained for particular temperatures and wave directions: for Si from Weber (1977), for SrTiO₃ from Yamada and Shirane (1969) and Cowley (1964), for KTaO₃ from Sahin and Dost (1988), and for Ge from Weber (1974).

Next, we describe the method of obtaining material parameters from experimental dispersion curves. We are concerned with isothermal static constants (independent of frequency). We assume, for example, the mechanical and the optical branch of shear wave dispersion curves $\omega(k)$ are given. We also assume as known, the lattice length a_0 , the mass density ρ and the dielectric susceptibility χ . The method has the following steps:

- 1) Focus in the region $0 \leq ka_0/\pi < 0.2$.
- 2) Arrange the mechanical branch as in Fig. 3a and find $c_s = d\omega/dk|_{k=0}$. As a result we find $c_{44} = c_s^2 \rho$.
- 3) From the initial curvature of the optical branch we find from Eq. (2.10) $\ell_s^2 = \Lambda_s/\Omega_s^2$.
- 4) Fit the mechanical branch according to Eq. (3.6) $\omega^2 = k^2 c_s^2 \ell_s^2 (k^2 + \ell_s^2)/(\ell_s^{-2} + (h_s^2/\ell_s^2)k^2)$, as suggested by Fig. 1a, and obtain h_s^2/ℓ_s^2 . As a result we calculate h_s^2 .

In case $\Lambda_s \approx 0$, from Fig. 1a we obtain $h_s = c_s/\max\omega$, where $\max\omega$ is the maximum mechanical frequency. Use fitting and obtain ℓ_s^2/h_s^2 and as a result calculate ℓ_s^2 .

- 1) Calculate $\alpha = 1/(\chi\epsilon_0)$.
- 2) From Eq. (2.30b) we find $(b_{44} + b_{77}) = ah_s^2$.
- 3) From Eq. (2.30a) we find $(e_{44} - f_{12})^2 = (h_s^2 - \ell_s^2)\alpha\mu$.

All the above steps can be performed in sequence and are robust regarding the obtainable parameters, avoiding complex and often ill-defined multivariable fittings. A similar task can be performed for the longitudinal (dilatational) dispersion modes. The set of all parameters are shown in [Table 3](#). Note that the parameter $(e_{44} - f_{12})$ as well as $(e_{11} - f_{11})$ can only be obtained as an absolute number. The sign was depicted if known from atomistic calculations; it is immaterial regarding the analysis. The computed result for $e_{44}-f_{12}$ for SrTiO_3 seems to be in good accord with the ab initio computations at 0 K of [Stengel \(2016\)](#) -1.96 V, of [Kvasov and Tagantsev \(2015\)](#) -1.5 V, of [Hong and Vanderbilt \(2013\)](#) -2.1 V. For Si, we quote the result of [Hong and Vanderbilt \(2013\)](#) -4.1 V. These results have remarkable similarity with our results given the simplicity of our model.

The above analysis holds for moderate wave numbers. For high wave numbers, the experimental dispersion curves show stronger nonlinearities that are related with the polarization inertia γ and the flexoelectric inertia M . The dynamic energy density can be extended to include these constants according to [Yuding and Tagatsev \(2013\)](#),

$$T = \frac{1}{2}\rho\dot{u}_i\dot{u}_i + \frac{1}{2}\gamma\dot{P}_i\dot{P}_i + M\dot{u}_i\dot{P}_i \quad (5.1)$$

We can approximate M and γ , by extending the present analysis as follows. A low bound polarization inertia $\text{min}\gamma$ can be found from [Shahin and Dost \(1988\)](#)

$$\text{min}\gamma = \frac{a}{\Omega_s^2} \quad (5.2)$$

An upper bound flexoelectric inertia $\text{max}|M|$ can be estimated from [Kvasov and Tagantsev \(2015\)](#)

$$\text{max}|M| = \sqrt{\rho\text{min}\gamma} \quad (5.3)$$

The computed bounds for M and γ have been included in [Table 3](#). They are in good accord with other values reported in the literature for SrTiO_3 (from [Kvasov and Tagantsev \(2015\)](#) $M = 8 \times 10^{-8} \text{Vs}^2/\text{m}^2$ at 0 K; from [Morozovska et al. \(2016\)](#) $M = 24 \times 10^{-8}$ at 120 K, $\gamma = 2.2 \times 10^{-17} \text{kgm}^3/\text{C}^2$ at 120 K).

6. Plane waves

Let us assume plane displacement waves (of direction \vec{d}) propagating with phase velocity c in a direction \vec{p} :

$$\begin{aligned} \vec{u} &= f(\vec{x} \cdot \vec{p} - ct)\vec{d} \\ \vec{P} &= g(\vec{x} \cdot \vec{p} - ct)\vec{d} \end{aligned} \quad (6.1)$$

\vec{d} , \vec{p} are unit vectors and $f(\vec{x} \cdot \vec{p} - ct)$, $g(\vec{x} \cdot \vec{p} - ct)$ are arbitrary functions of $(\vec{x} \cdot \vec{p} - ct)$. Without loss of generality, we will focus on plane problems (parallel to the $x_3 = 0$ plane) and decompose the fields according to the dilatation and deviatoric parts as in [Giannakopoulos and Rosakis \(2020\)](#), in the absence of body forces and initial electric field):

$$\begin{aligned} u_1(x_1, x_2, t) &= \frac{\partial\phi}{\partial x_1} + \frac{\partial H_3}{\partial x_2} \\ u_2(x_1, x_2, t) &= \frac{\partial\phi}{\partial x_2} - \frac{\partial H_3}{\partial x_1} \\ u_3(x_1, x_2, t) &= 0 \end{aligned} \quad (6.2)$$

with unknown potentials $\phi(x_1, x_2, t)$ and $H_3(x_1, x_2, t)$. Accordingly, the polarization vector is:

$$\begin{aligned} P_1(x_1, x_2, t) &= \frac{\partial\chi}{\partial x_1} + \frac{\partial K_3}{\partial x_2} \\ P_2(x_1, x_2, t) &= \frac{\partial\chi}{\partial x_2} - \frac{\partial K_3}{\partial x_1} \\ P_3(x_1, x_2, t) &= 0 \end{aligned} \quad (6.3)$$

with unknown potentials $\chi(x_1, x_2, t)$ and $K_3(x_1, x_2, t)$. The electric potential is $\Phi = \Phi(x_1, x_2, t)$.

The mechanical dynamic [Eqs. \(2.25\)](#) and [\(2.26\)](#) become:

$$\nabla^2\phi - \ell_p^2\nabla^4\phi = \frac{1}{c_p^2}\left(\ddot{\phi} - h_p^2\nabla^2\ddot{\phi}\right) \quad (6.4)$$

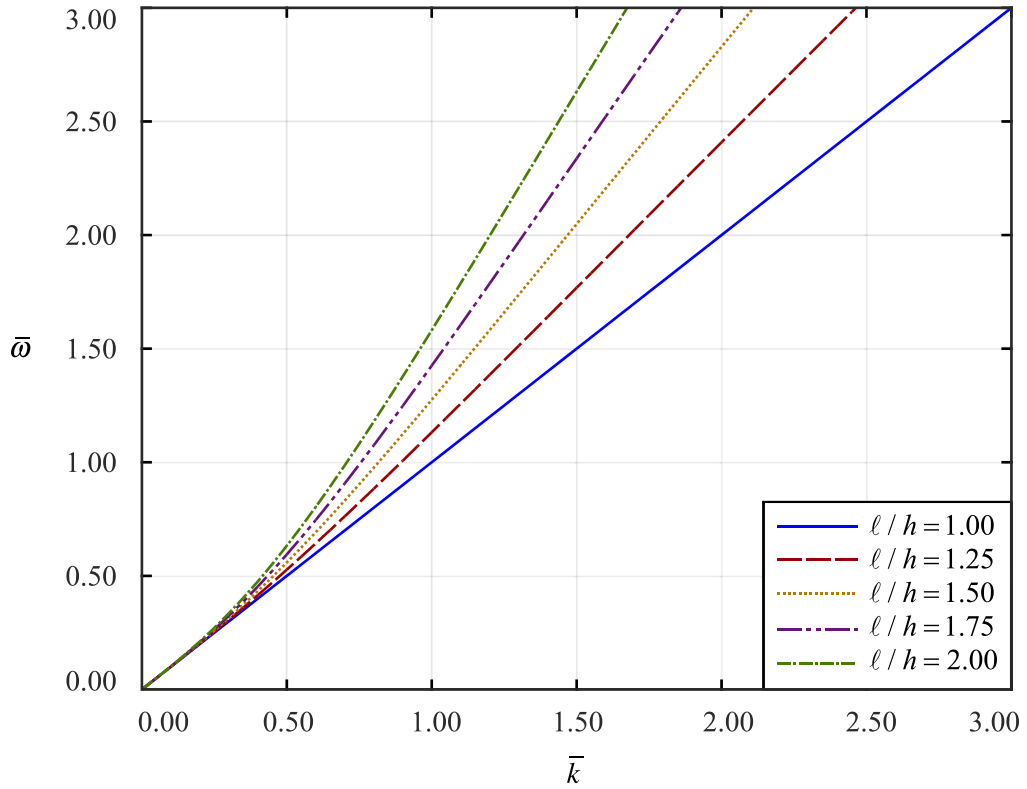


Fig. 5a. Normalized plot of the mechanical modes, implied by Eqs. (3.1) and (3.6) for the case of flexoelectric metamaterials $h_s / \ell_s \geq 1, h_p / \ell_p \geq 1$. The normalized frequency is $\bar{\omega} = \omega h_{p,s} / c_{p,s}$ and the normalized wave number is $\bar{k} = k h_{p,s}$. The suffix p and s denote dilatational and shear part respectively.

$$\nabla^2 H_3 - \ell_s^2 \nabla^4 H_3 = \frac{1}{c_s^2} \left(\ddot{H}_3 - h_s^2 \nabla^2 \ddot{H}_3 \right) \tag{6.5}$$

The polarization Eqs. (2.27) and (2.28) become:

$$\nabla^2 \chi - \ell_p^2 \nabla^4 \chi = \frac{1}{c_p^2} \left(\frac{e_{11} - f_{11}}{a + \varepsilon_0^{-1}} \nabla^2 \ddot{\phi} \right) \tag{6.6}$$

$$\nabla^2 K_3 - \ell_s^2 \nabla^4 K_3 = \frac{1}{c_s^2} \left(\frac{e_{44} - f_{12}}{a} \nabla^2 \ddot{H}_3 \right) \tag{6.7}$$

In the above equations, $\nabla^2 = \partial^2 / \partial x_1^2 + \partial^2 / \partial x_2^2$ is the two-dimensional Laplacian operator, and $\nabla^4 = \nabla^2 \nabla^2 = \partial^4 / \partial x_1^4 + 2 \partial^4 / \partial x_1^2 \partial x_2^2 + \partial^4 / \partial x_2^4$ is the two-dimensional biharmonic operator. When all micro-structural and micro-inertial lengths are zero, reduce to the plane stress classical elastodynamic equations, Achenbach (1990).

Substituting (6.1) into (6.4) and (6.6) we obtain for $\vec{d} \cdot \vec{p} = \pm 1$ (motion parallel to the wave propagation, i.e. longitudinal wave, + forward and - backward),

$$c^2 = c_p^2 \frac{\ell_p^2}{h_p^2} \leq c_p^2 \tag{6.8}$$

$$g' - \ell_p^2 g'' = \pm c_p^2 \frac{\ell_p^2}{h_p^2} \left(\frac{e_{11} - f_{11}}{a + \varepsilon_0^{-1}} \right) f'' \tag{6.9}$$

where (') denotes derivative with respect to $(\vec{x} \cdot \vec{p} - ct)$. For $(\vec{d} \times \vec{p})_3 = \pm 1$ (motion normal to the wave propagation, i.e. transverse or rotational wave + forward and - backward),

$$c^2 = c_s^2 \frac{\ell_s^2}{h_s^2} \leq c_s^2 \tag{6.10}$$

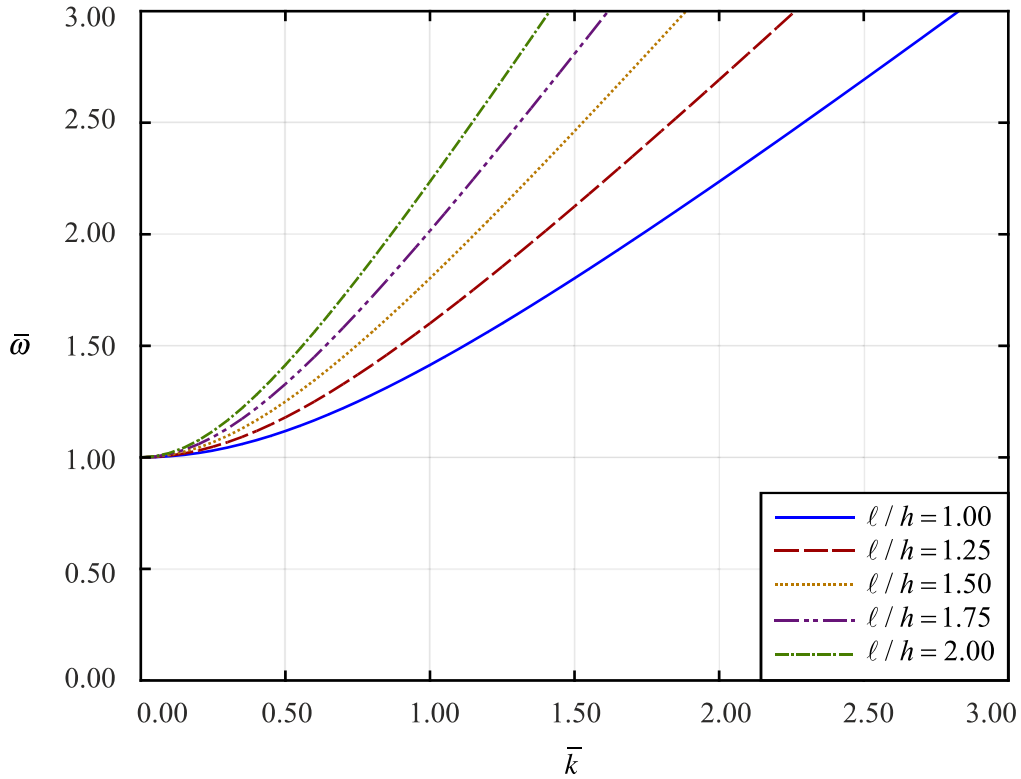


Fig. 5b. Normalized plot of the optical modes, implied by Eqs. (3.12) and (3.14) for the case of flexoelectric metamaterials $h_s / \ell_s \geq 1, h_p / \ell_p \geq 1$. The normalized frequency is $\bar{\omega} = \omega / \Omega_{p,s}$ and the normalized wave number is $\bar{k} = kh_{p,s}$. The suffix p and s denote dilatational and shear part respectively.

$$g' - \ell_s^2 g'' = \pm c_s^2 \frac{\ell_s^2}{h_s^2} \left(\frac{e_{44} - f_{12}}{a} \right) f'' \tag{6.11}$$

Note that the longitudinal (6.8) and transverse (6.10) velocities of the plane waves were found to depend on the corresponding microstructural lengths and are less of equal to the classic plane wave velocities.

6.1. Time-harmonic plane waves

Let us now consider time-harmonic plane waves by letting the vectors \vec{d}, \vec{p} be either real or imaginary so that $\vec{d} \cdot \vec{p} = \text{real}$. The functions f and g particularize to:

$$\begin{aligned} f &= A \exp \left[ik \left(\vec{x} \cdot \vec{p} - \frac{\omega}{k} t \right) \right] \\ g &= B \exp \left[ik \left(\vec{x} \cdot \vec{p} - \frac{\omega}{k} t \right) \right] \end{aligned} \tag{6.12}$$

where A and B are real or imaginary constants with $A \vec{d} = \text{real}, B \vec{d} = \text{real}$ and k the wave number (complex in general). Denote by $\omega = kc$ the circular frequency (real), related to a time period $2\pi/\omega$.

Replacing (6.12) in (6.4) and (6.5), we obtain:

$$\left(\frac{\omega}{k} \right)_p^2 = c_p^2 \left(\frac{1 + \ell_p^2 k^2}{1 + h_p^2 k^2} \right) \tag{6.13}$$

for the longitudinal waves and

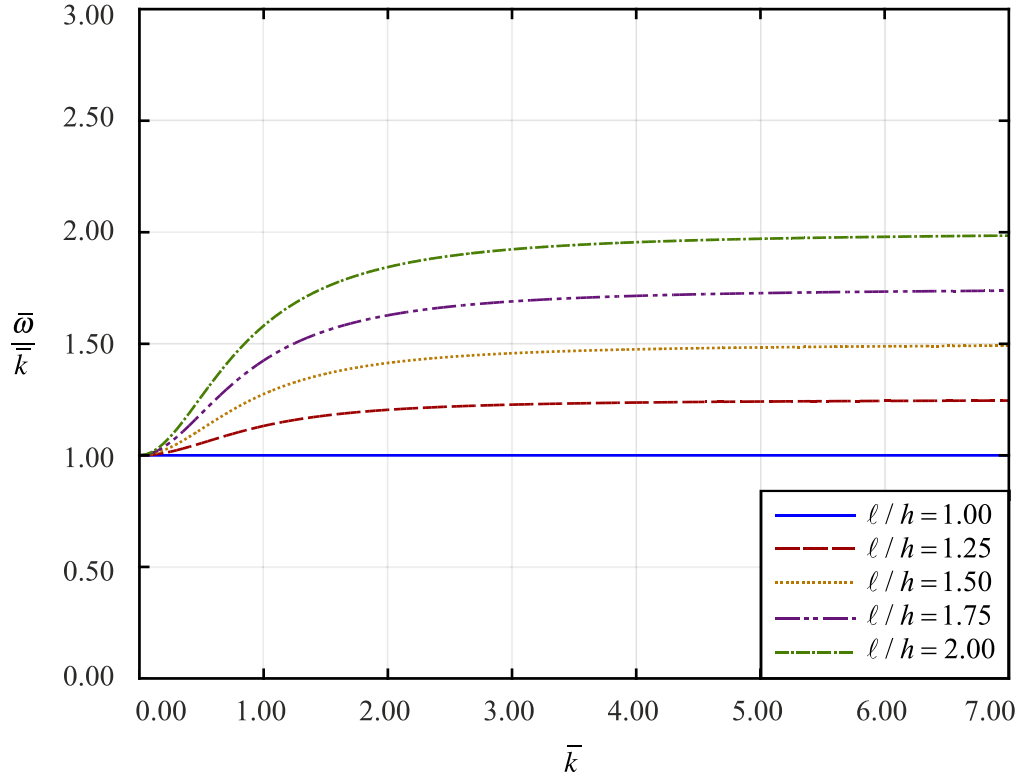


Fig. 6a. Normalized *mechanical phase velocity* $\bar{\omega}/\bar{k}$, as a function of the normalized wave number \bar{k} for the case of flexoelectric metamaterials $h_s/\ell_s \geq 1, h_p/\ell_p \geq 1$. The normalization is as in Fig. 4.

$$\left(\frac{\omega}{k}\right)_s^2 = c_s^2 \left(\frac{1 + \ell_s^2 k^2}{1 + h_s^2 k^2} \right) \quad (6.14)$$

for the transverse waves. These results are the same as (3.1) and (3.6).

Replacing (6.12) in (6.9) and (6.11), we obtain:

$$B(1 + \ell_p^2 k^2) = \mp \left(\frac{e_{11} - f_{11}}{a + \varepsilon_0^{-1}} \right) A \omega^2 \quad (6.15)$$

which is the same as (3.12) for the longitudinal waves.

Replacing (6.12) in (6.10) and (6.12), we obtain:

$$B(1 + \ell_s^2 k^2) = \mp \left(\frac{e_{44} - f_{12}}{a} \right) A \omega^2 \quad (6.16)$$

which is the same as (3.16) for the transverse waves.

7. Flexoelectric metamaterials

The previous analysis has been based on the assumption the dielectric susceptibility is positive $\chi > 0$, hence $a > 0$. This assumption seems to be true for all known homogeneous dielectrics. The positive value of susceptibility leads to the fact that the ratios of the microinertial to the microstructural lengths is greater than one, $h_s/\ell_s \geq 1, h_p/\ell_p \geq 1$. This result stems from Eqs. (2.30) and (2.31).

However, Verago (1968) pointed out the possibility of negative electric susceptibility $\chi < 0$, hence $a < 0$, but it was realized that at the time there was no such materials, natural or artificial. In recent years, synthetic materials have appeared that show negative electric susceptibility and have been termed as *dielectric metamaterials*, see for example Koo (2015). Optical metamaterials can be considered as flexoelectric metamaterials which can be regarded as effective media with simultaneously negative electric permittivity and negative magnetic permeability and thus an effectively negative refractive index, Lu et al. (2009). In such cases, Eqs. (2.30) and (2.31) indicate that $h_s/\ell_s < 1, h_p/\ell_p < 1$. This possibility for flexoelectric metamaterials was realized first by Giannakopoulos and Zisis (2020). Other flexoelectric metamaterials can be composites of dielectric matrix with aligned metal fibres (see for example related reviews of Padilla et al. (2006) and Smith et al. (2004)).

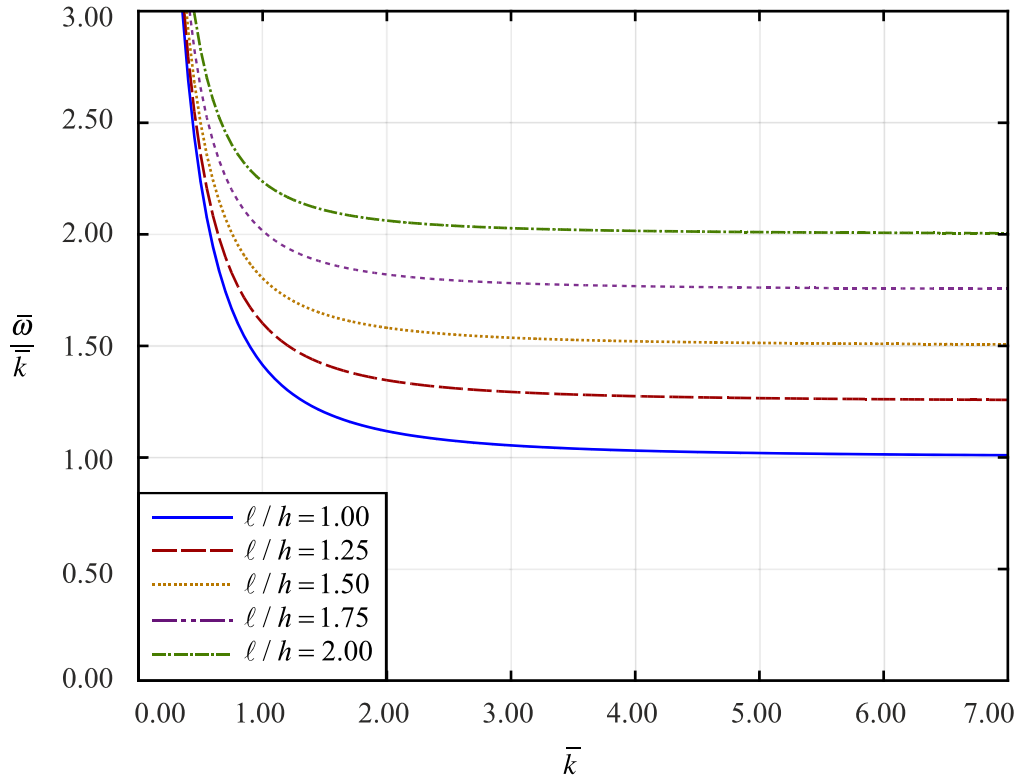


Fig. 6b. Normalized optical phase velocity $\bar{\omega}/\bar{k}$, as a function of the normalized wave number \bar{k} for the case of flexoelectric metamaterials $h_s/\ell_s \geq 1, h_p/\ell_p \geq 1$. The normalization is as in Fig. 4.

The first generation of optical negative index metamaterials were constructed from a printed (shadow mask/etching) circuit board material of fiber glass, with regular arrays of copper split-ring resonators (SRR) (see, for example, Shelby et al. (2001)). The SRR concept was originally introduced by Pendry et al. (1999): the two metal micro-rings form the inductances and the two slits as well as the gap between the two rings form the capacitors, with the electric field being parallel to the SRR plane. Negative refractive index of metal–dielectric composites has been suggested by Kildishev et al. (2006), with a simple structure consisting of a periodic array of identical gold strips. Clearly, it is not the scope of the present work to include all the research that has been carried out with respect to the field of composite optical metamaterials. It suffices to point that these composites include ever smaller metal particles in various dielectric matrices (mainly plastics), which are to be used in high-frequency applications.

The longitudinal (6.8) and transverse (6.10) velocities of the plane waves was found to depend on the corresponding micro-structural lengths and are less than or equal to the classic plane wave velocities because the micro-inertial lengths are greater than or equal to the micro-structural length. The opposite effect is expected when we encounter flexoelectric metamaterials in which case the micro-inertial lengths are less than the micro-structural length.

Fig. 5a shows the normalized plot of the mechanical modes, implied by Eqs. (3.1) and (3.6) for the case of flexoelectric metamaterials $h_s/\ell_s \geq 1, h_p/\ell_p \geq 1$. Fig. 5b shows the normalized plot of the optical modes, implied by Eqs. (3.12) and (3.14). The normalized wave number is $\bar{k} = kh_{p,s}$. The suffix p,s denotes dilatational and shear part accordingly. The normalized frequency for the mechanical modes is $\bar{\omega} = \omega h_{p,s}/c_{p,s}$. The normalized frequency for the optical modes is $\bar{\omega} = \omega/\Omega_{p,s}$. Note the anomalous dispersion curves that appear (comparing with the results of Fig.1).

Fig. 6a shows the normalized mechanical phase velocity $\bar{\omega}/\bar{k}$, as a function of the normalized wave number \bar{k} for the case of flexoelectric metamaterials. Fig. 6b shows the normalized optical phase velocity $\bar{\omega}/\bar{k}$, as a function of the normalized wave number \bar{k} for the case of flexoelectric metamaterials. Fig. 7a shows the normalized mechanical group velocity $d\bar{\omega}/d\bar{k}$, as a function of the normalized wave number \bar{k} . Fig. 7b shows the normalized optical group velocity $d\bar{\omega}/d\bar{k}$, as a function of the normalized wave number \bar{k} . From Fig. 7a we can observe that the group velocity increases up to a maximum value and then decreases towards a lower asymptote. This indicates that backward waves (group velocity opposite to phase velocity) are possible in such media, as has been found in wave guides (plates and cylinders), Meitziel (1965).

Regarding the mechanical phase velocity, we observe the analogy with the phase velocity that is encountered in the dynamic behavior of a Zener type (standard) viscoelastic model, Carcione (2007). Viscoelasticity shows anomalous dispersion curves like the ones shown by the flexoelectric metamaterials. The phase velocity $c_{ph} = \omega/k$ for the simple shear wave traveling in the standard viscoelastic solid, normalized by the shear wave speed c_s is given by

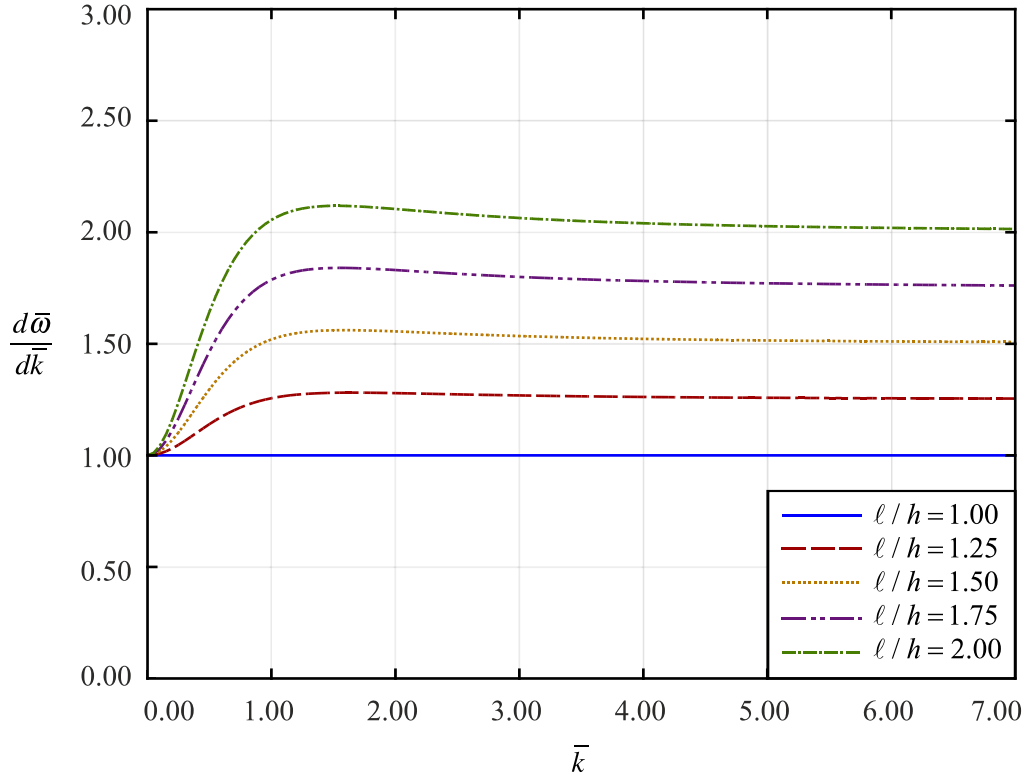


Fig. 7a. Normalized mechanical group velocity $d\bar{\omega}/d\bar{k}$, as a function of the normalized wave number \bar{k} for the case of flexoelectric metamaterials $h_s/\ell_s \geq 1, h_p/\ell_p \geq 1$. The normalization is as in Fig. 4.

$$\frac{(\omega/k)}{c_s} = \text{Re} \left[\sqrt{\frac{1 + i\omega\tau_\varepsilon}{1 + i\omega\tau_\sigma}} \right] \quad (7.1)$$

where $i = \sqrt{-1}$, ω is the frequency, k is the wave length and $\tau_\varepsilon \geq \tau_\sigma > 0$ are the relaxation times. It is easy to show that the analogy with Eq. (3.7) requires

$$\frac{\ell_s}{h_s} = \frac{\tau_\sigma}{\tau_\varepsilon} \geq 1 \quad (7.2)$$

Therefore the flexoelectric metamaterial model is analogous to the Zener viscoelastic model, with Eq. (7.2) describing the parameter equivalence.

8. Conclusions

We have extended our flexoelectric analysis and investigated the dispersion relations and found that for each, dilatational and shear, mechanical types of waves, two coupled branches appear: an acoustic and an optical one that approximate well the experimental results for many flexoelectric materials. Each dispersion relation (dilatational and shear) is affected strongly by both the microstructural and the micro-inertial length. These dispersion relations are not expected in classical elasto-dynamics where the absence of internal lengths leads to no dispersion. Moreover, we have investigated the role of the group velocity as a velocity of energy transport and showed that it also has dispersive character; in contrast to the classic case that shows no dispersion (group velocities are identical to the phase velocities). This is a new but expected result. A notable similarity with classic elasto-dynamics is that the plane waves are also partitioned to longitudinal and transverse waves with distinct dispersion relations and group velocities. The present results fall back to the classic case in absence of the flexoelectric related microlengths. The optical branch of the dispersion relation appears due to the polarization field that accompanies the mechanical field. The longitudinal and transverse velocities of the plane waves depend on the corresponding microstructural lengths and are less than or equal to the classic plane wave velocities. Moreover, we prove that the energy and the wave lengths travel with the group velocity. A major application that has motivated the present work is related to the near fault motion signatures associated with sub-Rayleigh and supershear rupture growth along material interfaces as well as natural geological faults. We are interested in both signals generated by “real” earthquakes and in ones generated by the growth of dynamic shear ruptures at the frictional interfaces between flexoelectric Polymers (Laboratory earthquakes). We note here that both crustal rocks (e.g. MgO) and many polymers (e.g. PMMA) are known to be flexoelectric.

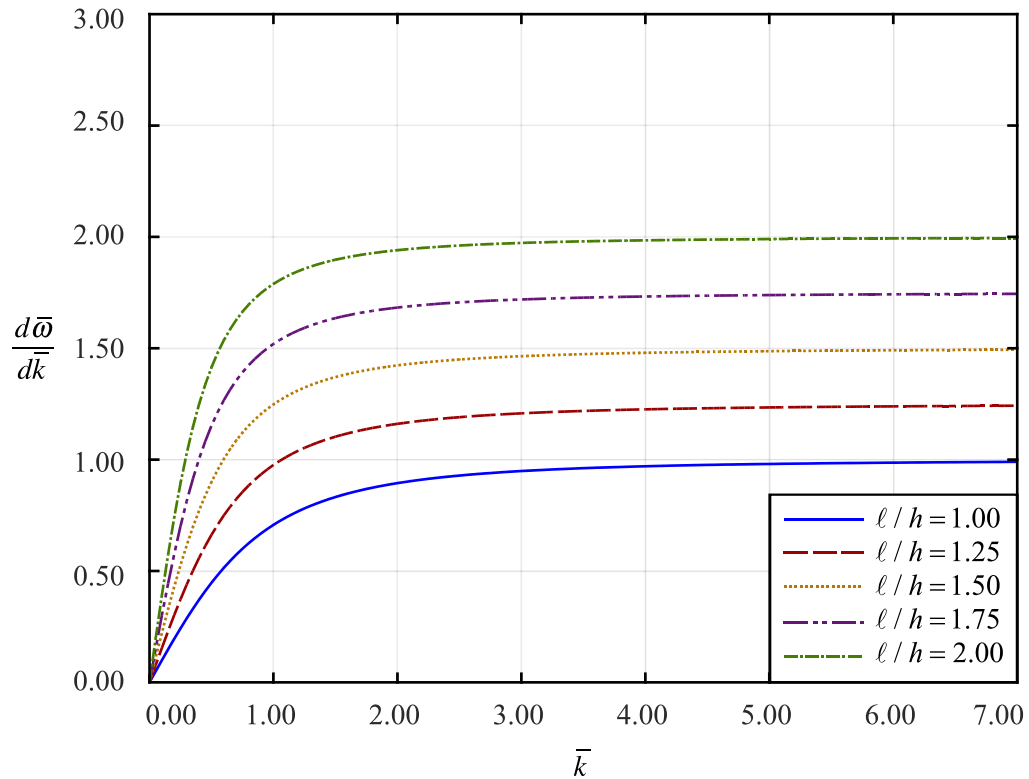


Fig. 7b. Normalized optical group velocity $d\bar{\omega}/d\bar{k}$, as a function of the normalized wave number \bar{k} for the case of flexoelectric metamaterials $h_s/\ell_s \geq 1$, $h_p/\ell_p \geq 1$. The normalization is as in Fig. 4.

Our dispersion relations resemble the dispersion of structural wave guides like circular cylinders and plates when investigated by classic elasto-dynamics. In the later cases the characteristic lengths are macroscopic dimensions of waveguides like the cylinder radius and the plate thickness. A new result that has no analogy with classical elastodynamics is the possibility of evanescent bulk waves that can coexist with traveling waves. Such waves are expected at reflection and transmission of waves on material interfaces and free surfaces. More investigations are expected along these lines.

The dispersion relations (mechanical and optical) were found to correlate well with available experimental results from neutron scattering for moderate wavenumbers. We presented a methodology that can be used to obtain flexoelectric properties by fitting the analytical results to both the mechanical and the optical branches of the shear wave experimental dispersion curves, and obtained reasonably good material parameters. We can conclude that the proposed continuum, simple dynamic flexoelectric theory can serve well as an approximation for moderate wave numbers and frequencies. The theory is not adequate for high wave numbers and frequencies, but this is not a major limitation for many engineering problems such as dynamic fracture.

An interesting analogy has been established between viscoelastic models and flexoelectric metamaterials. Flexoelectric metamaterials accept negative sign of the dielectric constant (accompanied by a similar change of sign of the magnetic permeability) and could lead to anomalous dispersion curves, just as the ones predicted by the viscoelastic models. The analogy is based on the ratio of the micro-structural versus the micro-inertia lengths that corresponds to the ratio of the characteristic times of viscoelasticity (creep/relaxation).

The results are important for all dielectrics such as ceramics, ice, perovskites and polymers that exhibit strong flexoelectric effect, often uncoupled from piezoelectricity (centrosymmetric materials). However, the results also apply to nano-composite and atomistic models that can be approached in the context of couple stress elasticity. In such cases, the origin of the micro-structural and micro-inertial lengths is very different that the one proposed in this work.

CRediT authorship contribution statement

Antonios E. Giannakopoulos: Conceptualization, Methodology, Investigation, Writing – original draft, Writing – review & editing, Formal analysis. **Ares J. Rosakis:** Conceptualization, Methodology, Investigation, Writing – original draft, Writing – review & editing, Formal analysis.

Declaration of competing interest

The authors declare that they have no known competing financial interests or personal relationships that could have appeared to influence the work reported in this paper.

Data availability

Data will be made available on request.

Acknowledgements

With gratitude to our mentor, Professor L. B. Freund, who taught us all we know on Elastodynamics. A. J. R. acknowledges support from the US Geological Survey (USGS) (grand No. G20AP0037) and from the 2019 Caltech/MCE Big Idea Fund (BIF).

Appendix A. Necessary conditions for separation of variables

In this Appendix we provide the necessary conditions required by the assumption of separation of space and time variables in the dispersion relations. Assume, without loss of generality, that the dilatational Helmholtz potential can be written as $\phi(\vec{x}, t) = \phi^t(t)\phi^x(\vec{x})$. Inserting this decomposition in Eq. (6.5), we obtain

$$\left(\nabla^2\phi^x - \ell_p^2\nabla^4\phi^x\right)\phi^t = \frac{1}{c_p^2}\left(\ddot{\phi}^x - h_p^2\nabla^2\ddot{\phi}^x\right)\ddot{\phi}^t \tag{A.1}$$

From standard mathematical procedures, we may rearrange (A.1) as

$$\frac{\left(\nabla^2\phi^x - \ell_p^2\nabla^4\phi^x\right)}{\left(\phi^x - h_p^2\nabla^2\phi^x\right)}c_p^2 = \frac{\ddot{\phi}^t}{\phi^t} = -\omega^2 \tag{A.2}$$

where ω is a real frequency type parameter that keeps the solution bounded. Therefore,

$$\phi^t = C\exp(-i\omega t) + D\exp(i\omega t) \tag{A.3}$$

where C and D are constants [m^2] and

$$\left(\nabla^2\phi^x - \ell_p^2\nabla^4\phi^x\right) + \frac{\omega^2}{c_p^2}\left(\phi^x - h_p^2\nabla^2\phi^x\right) = 0 \tag{A.4}$$

If we assume that the spatial solution can be analyzed with a Fourier series, then a typical term can be assumed as $\phi^x(\vec{x}) \approx A\exp[ik(\vec{n} \cdot \vec{x})] + B\exp[-ik(\vec{n} \cdot \vec{x})]$ where k is a wave number, \vec{n} is the direction of the traveling wave and A, B are constants [m^2]. Inserting this in eq. (A.4), we obtain

$$\frac{\omega^2}{c_p^2}\left(1 + h_p^2k^2\right) = k^2\left(1 + \ell_p^2k^2\right) \tag{A.5}$$

which is nothing but the dispersion relation (3.1). In conclusion, the form of the plane waves requires the frequency ω to be real and the spatial resolution of the solution to be expandable in Fourier series.

Appendix B. The group velocity as an energy transport velocity

In this Appendix we show that the mechanical group velocities (Eq. (3.26)) are the velocities of the transfer of the time average of the power per unit area. The time average over a period $\omega/2\pi$ of the power per unit area of the advancing wave plane is:

$$\langle \wp \rangle = -\frac{\omega}{2\pi} \int_0^{2\pi/\omega} \left(t_i \dot{u}_i + r_i p_j \frac{\partial \dot{u}_i}{\partial x_j} + p_i E_{ij} \dot{P}_j \right) dt \tag{B.1}$$

where

$$\begin{aligned} t_i &= \sigma_{ij}p_j - \tau_{kji,k}p_j + (D_1n_i)p_jp_k\tau_{kji} - D_j(\tau_{kji}p_k) \\ D_j &= (\delta_{jk} - p_jp_k)\partial/\partial x_k \end{aligned} \tag{B.2}$$

$$r_i = \tau_{kji}p_kp_j \tag{B.3}$$

$$E_{ij} = b_{ijkl}P_{l,k} + e_{ijkl}\epsilon_{kl} + b_{ij}^0 \tag{B.4}$$

The corresponding time average of the internal energy density and the kinetic energy density is $\langle W \rangle + \langle T \rangle = 2\langle T \rangle$ in the absence of energy dissipation. The time average of the kinetic energy is:

$$\langle T \rangle = \frac{\omega}{2\pi} \int_0^{2\pi/\omega} \left(\frac{1}{2} \rho \dot{u}_i \dot{u}_i \right) dt \tag{B.5}$$

Then, the velocity of the energy transport by plane time-harmonic waves c_e is defined as:

$$\langle \wp \rangle = 2\langle T \rangle c_e \tag{B.6}$$

Without loss of generality we utilize the results of Section 6.1 and replace them in the above equations. After a lengthy but straightforward algebra, we obtain for the longitudinal waves:

$$c_e = c_p \left(1 + \ell_p^2 k^2 \right)^{1/2} \left(1 + h_p^2 k^2 \right)^{-1/2} + c_p \left(\ell_p^2 k^2 - h_p^2 k^2 \right) \left(1 + \ell_p^2 k^2 \right)^{-1/2} \left(1 + h_p^2 k^2 \right)^{-3/2} \tag{B.7}$$

and

$$c_e = c_s \left(1 + \ell_s^2 k^2 \right)^{1/2} \left(1 + h_s^2 k^2 \right)^{-1/2} + c_s \left(\ell_s^2 k^2 - h_s^2 k^2 \right) \left(1 + \ell_s^2 k^2 \right)^{-1/2} \left(1 + h_s^2 k^2 \right)^{-3/2} \tag{B.8}$$

for the tangential waves. These results are identical with the group velocity results found in Eqs. (3.3) and (3.8) respectively. Thus, for the mechanical dispersion relations we proved that

$$c_e = \left(\frac{d\omega}{dk} \right)_{p,s} \tag{B.9}$$

Appendix C. The group velocity as a wavelength transport velocity

In this Appendix we will show that the wavelengths propagate with the group velocity. In order to simplify the discussion, assume plane waves traveling in the x direction and wave lengths $1/k$ corresponding to real wave numbers. Assume that frequency and wave number are functions of x and t. Conservation of wave crests imply (Rossby, 1945)

$$\frac{\partial k}{\partial t} + \frac{\partial \omega}{\partial x} = 0 \tag{C.1}$$

Denote the phase velocity as $c = \omega/k$. Then (C.1) becomes

$$\frac{\partial}{\partial t} \left(\frac{1}{k} \right) + \left(c - \frac{1}{k} \frac{c}{(1/k)} \right) \frac{\partial}{\partial x} \left(\frac{1}{k} \right) = 0 \tag{C.2}$$

The group velocity can be defined as

$$c_g = c - \frac{1}{k} \frac{c}{(1/k)} \tag{C.3}$$

We can also show that

$$c_g = c + k \frac{\partial c}{\partial k} = \frac{c^2}{c - \omega \frac{\partial c}{\partial \omega}} \tag{C.4}$$

Indeed, Eq. (C.4) gives the same result as Eq. (3.26). Note that to have positive group velocity

$$c > \omega \frac{\partial c}{\partial \omega} \tag{C.5}$$

which is true for our present flexoelectric model. Also, if $\frac{\partial c}{\partial \omega} \geq 0$ then $c \geq c_g$ (the phase velocity is larger than the group velocity), as happens in our case.

From Eq. (C.2) we can find a phase function $\psi(x, t)$ such that

$$\omega = \frac{\partial \psi}{\partial t}, \quad \frac{1}{k} = -\frac{\partial \psi}{\partial x} \tag{C.6}$$

which implies that $c_g = \frac{\partial \omega}{\partial k}$ as usually taken for group velocity. Therefore, Eq. (C.6) proves that the wavelength can propagate with the group velocity without distortion $1/k = f(x - c_g t)$.

References

- Achenbach, J.D., 1990. Wave Propagation in Elastic Solids. North-Holland Publications.
- Askar, A., Lee, P.C.Y., Cakmak, A.S., 1970. Lattice-dynamics approach to the theory of elastic dielectrics with polarization gradient. *Phys. Rev. B* 1, 3525–3537.
- Axe, J.D., Harado, J., Shirane, G., 1970. Anomalous acoustic dispersion in centrosymmetric crystals with soft optic phonons. *Phys. Rev. B* 1, 1227–1234.
- Barrett, J.H., 1952. Dielectric constant in perovskite type crystals. *Phys. Rev.* 86, 118–120.
- Ben-Amoz, M., 1976. A dynamic theory for composite materials. *J. Appl. Math. Phys. (ZAMP)* 27, 83–99.
- Brillouin, L., 1946. Wave Propagation in Periodic Structures. McGraw-Hill, New York.
- Carcione, J.M., 2007. Wave Fields in Real Media: Wave Propagation in Anisotropic, Anelastic, Porous and Electromagnetic Media: Third Edition Chapter 2. Viscoelasticity and Wave Propagation. Elsevier, pp. 51–95.
- Coak, M.J., Haines, C.R.S., Liu, C., Guzman-Verri, G.G., Saxena, S.S., 2019. Pressure dependence of ferroelectric quantum critical fluctuations. *Phys. Rev. B* 100, 214111.
- Codony, D., Mocchi, A., Barcelo-Mercader, J., Arias, I., 2021. Mathematical and computational modelling of flexoelectricity. *J. Appl. Phys.* 130, 231102.
- Cowley, R.A., 1964. Lattice dynamics and phase transitions of strontium titanate. *Phys. Rev.* 134, A981–A997.
- Dell'Isola, F., Madeo, A., Placidi, L., 2012. Linear plane wave propagation and normal transmission and reflection at discontinuity surfaces in second gradient 3D continua. *Z. Angew. Math. Mech.* 92, 52–71.
- Engelbrecht, J., Berezovski, A., Pastrone, F., Braum, M., 2005. Waves in microstructural materials and dispersion. *Philosoph. Mag.* 85, 4127–4141.
- Gavardinas, I.D., Giannakopoulos, A.E., Zisis, Th., 2018. A von Karman plate analogue for solving anti-plane problems in couple stress and dipolar gradient elasticity. *Int. J. Solids Struct.* 148–149, 169–180.
- Georgiadis, H.G., Vardoulakis, I., Velgaki, E.G., 2004. Dispersive Rayleigh-wave propagation in microstructural gradient elasticity. *J. Elasticity* 74, 17–45.
- Giannakopoulos, A.E., Rosakis, A.J., 2022. Dynamic magneto-flexoelectricity and seismo-electromagnetic phenomena: connecting mechanical response to electromagnetic signatures. *J. Mech. Phys. Solids* 168, 105058.
- Giannakopoulos, A.E., Rosakis, A.J., 2020. Dynamics of flexoelectric materials: subsonic, intersonic and supersonic ruptures and Mach cone formation. *J. Appl. Mech. ASME* 87, 061004-1/9.
- Giannakopoulos, A.E., Zisis, Th., 2019. Uniformly moving screw dislocation in flexoelectric materials. *Eur. J. Mech. / A Solids* 78–149, 103843.
- Giannakopoulos, A.E., Zisis, Th., 2020. Uniformly moving antiplane cracks in flexoelectric materials. *Eur. J. Mech. / A Solids*, 85–104136.
- Giannakopoulos, A.E., Zisis, Th., 2021. Steady-state antiplane crack considering the flexoelectric effect: surface waves and flexoelectric metamaterials. *Arch. Appl. Mech.* 10, 1007.
- Gouriots, P.A., Georgiadis, H.G., 2017. Torsional and SH waves in an isotropic and homogeneous elastic half-space characterized by the Toupin-Mindlin gradient theory. *Int. J. Solids Struct.* 62, 217–228.
- Harada, J., Axe, J.D., Shirane, G., 1971. Neutron-scattering study of soft modes in cubic BaTiO₃. *Phys. Rev. B* 4, 155–162.
- Hong, J., Vanderbilt, D., 2013. First-principles theory and calculation of flexoelectricity. *Phys. Rev. B* 88, 174107.
- Hu, Y.W., Liang, X., Shen, S., 2018. Wave propagation in flexoelectric microstructured solids. *J. Elasticity* 130, 197–210.
- Hu, S., Shen, S., 2010. variational principles and governing equations in nano-dielectrics with the flexoelectric effect. *Sci. China Phys., Mech. Astron.* 53, 1497–1504.
- Huller, A., 1969. Soft phonon dispersion in BaTiO₃. *Z. Physik* 220, 145–158.
- Jackson, J.D., 1975. Classical Electrodynamics. John Wiley & Sons, New York.
- Kaplunov, J.D., Nolde, E.V., Rogerson, G.A., 2000. A low-frequency model for dynamic motion in prestressed incompressible elastic structures. *Proc. R. Soc. London* A456, 2589–2610.
- Kildishev, A.V., Cai, W., Chettiar, U.K., Yuan, H.K., Sarychev, A.K., Drachev, V.P., Shalae, V.M., 2006. Negative refractive index in optics of metal-dielectric composites. *JOSA B* 23 (3), 423–433.
- Koo, J.H., 2015. Negative electric susceptibility and magnetism from translational invariance and rotational invariance. *J. Magn. Magn. Mater.* 375, 106–110.
- Krichen, S., Sharma, P., 2016. Flexoelectricity: a perspective on an unusual electromechanical coupling. *J. Appl. Mech.* 83, 030801.
- Kittel, C., 1971. Introduction to Solid State Physics. Wiley, New York.
- Kvasov, A., Tagantsev, A.K., 2015. Dynamic flexoelectric effect in perovskites from first-principles calculations. *Phys. Rev. B* 92, 054104.
- Lu, M.H., Feng, L., Chen, Y.F., 2009. Phononic crystals and acoustic metamaterials. *Mater. Today* 12 (12), 34–42.
- Liu, C., Hu, S., Shen, S., 2014. Effect of flexoelectricity on band structures of one-dimensional phononic crystals. *J. Appl. Mech.* 81, 051007.
- Ma, W., Cross, L.E., 2006. Flexoelectricity of barium titanate. *Appl. Phys. Lett.* 88, 232902.
- Maranganti, R., Sharma, N.D., Sharma, P., 2006. Electromechanical coupling in non-piezoelectric materials due to nanoscale nonlocal size effects: green's functions and embedded inclusions. *Phys. Rev. B* 74, 014110. Erratum: Piezoelectric thin-film super-lattices without using piezoelectric materials [*J. Appl. Phys.* 108, 024304 (2010)] N. D. Sharma, C. Landis, and P. Sharma.
- Maranganti, R., Sharma, P., 2009. Atomistic determination of flexoelectric properties of crystalline dielectrics. *Phys. Rev. B* 80, 054109.
- Meitzler, A.H., 1965. Backward-wave transmission of stress pulses in elastic cylinders and plates. *J. Acoust. Soc. Am.* 38, 835–842.
- Mello, M., Bhat, H.S., Rosakis, A.J., Kanamori, H., 2014. Reproducing the supershear portion of the 2002 Denali earthquake rupture in laboratory. *Earth Planet. Sci. Lett.* 384, 89–96.
- Mello, M., Bhat, H.S., Rosakis, A.J., Kanamori, H., 2010. Identifying the unique ground motion signatures of supershear earthquakes: theory and experiments. *Tectonophysics* 493, 297–326.
- Mindlin, R.D., 1963. Micro-structure in linear elasticity. *Arch. Rational Mech. Anal.* 16, 51–78.
- Mindlin, R.D., 1968. Polarization gradient in elastic dielectric. *Int. J. Solids Struct.* 4, 637–642.
- Mindlin, R.D., 1969. Continuum and lattice theories of influence of electromechanical coupling on capacitance of thin dielectric films. *Int. J. Solids Struct.* 5, 1197–1208.
- Mizzi, C.A., Guo, B., Marks, L.D., 2022. experimental determination of flexoelectric coefficients in SrTiO₃, KTaO₃, TiO₂ and YAlO₃ single crystals. *Phys. Rev. Mater.* 6, 055005.
- Morozovska, A., Eliseev, E.A., Scherbakov, C.V., Vysochanskii, Y.M., 2016. Influence of elastic strain gradient on the upper limit of flexocoupling strength, spacially modulated phases, and soft phonon dispersion in ferroics. *Phys. Rev. B* 94, 174112.
- Nobili, A., Radi, E., Signorini, C., 2019. A new Rayleigh-like wave in guided propagation of antiplane waves in couple stress materials. *Proc. R. Soc. A* 476, 2019822.
- Padilla, W.J., Basov, D.N., Smith, D.R., 2006. Negative refractive index metamaterials. *Mater. Today* 9, 28–35.
- Papargyri-Beskou, S., Polyzos, D., Beskos, D.E., 2009. Wave dispersion in gradient elastic solids and structures: a unified treatment. *Int. J. Solids Struct.* 46, 3751–3759.
- Pendry, J.B., Holden, A.J., Robbins, D.J., Stewart, W.J., 1999. Magnetism from conductors and enhanced nonlinear phenomena. *IEEE Trans. Microwave Theory Tech.* 47 (11), 2075–2084.
- Pouget, J., Maugin, G.A., 1980. Coupled acoustic-optic modes in deformable ferroelectrics. *J. Acoust. Soc. Am.* 68, 588–601.
- Qu, Y., Jin, F., Yang, J., 2021a. Flexoelectric effects in second-order extension of rods. *Mech. Res. Commun.*, 103625.
- Qu, Y., Jin, F., Yang, J., 2021b. Torsion of a flexoelectric semiconductor rod with a rectangular cross section. *Arch. Appl. Mech.* <https://doi.org/10.1007/s00419-020-01867-0>.
- Raunio, G., Almqvist, L., 1969. Dispersion relations for phonons in KCl at 80 and 300 K. *Phys. Stat. Sol.* 33, 209–215.
- Raunio, G., Alqvist, L., Stedman, R., 1969. Phonon dispersion relations in NaCl. *Phys. Rev.* 178, 1496–1501.
- Rosby, C.-G., 1945. On the propagation of frequencies and energies in certain type of oceanic and atmospheric waves. *J. Meteorol.* 2, 187–204.1.
- Sannikov, D.G., 1962. Dispersion in ferroelectrics. *J. Exp. Theoretical Phys.* 14, 98–101.
- Santosa, F., Symes, W.W., 1991. A dispersive effective medium for wave propagation in periodic composites. *SIAM J. Appl. Math.* 51, 984–1005.

- Shahin, E., Dost, S., 1988. A strain-gradient theory of elastic dielectrics with dispersion. *Int. J. Engng. Sci.* 26, 1231–1245.
- Sharma, N.D., Landis, C.M., Sharma, P., 2010. Piezoelectric thin-film superlattices without using piezoelectric materials. *J. Appl. Phys.* 108, 024304.
- Sharma, N.D., maranganti, R., Sharma, P., 2007. On the possibility of piezoelectric nanocomposites without using piezoelectric materials. *J. Mech. Phys. Solids* 55, 2328–2350.
- Shelby, R.A., Smith, D.R., Nemat-Nasser, S.C., Schultz, S., 2001. Microwave transmission through a two-dimensional, isotropic, left-handed metamaterial. *Appl. Phys. Lett.* 78 (4), 489–491.
- Shirane, G., Axe, J.D., Harada, J., Remeika, J.P., 1970. Soft ferroelectric modes in lead titanate. *Phys. Rev. B* 2, 155–159.
- Shu, L., Wei, X., Pang, T., Yao, X., Wang, C., 2011. Symmetry of flexoelectric coefficients in crystalline medium. *J. Appl. Phys.* 110, 104106.
- Shirana, G., Nathane, R., Minkiewicz, V.J., 1967. Temperature dependence of the soft ferroelectric mode in KTaO_3 . *Phys. Rev.* 157, 396–399.
- Smith, D.R., Pendry, J.B., Wiltshire, M.C.K., 2004. Metamaterials and negative refractive index. *Science* 305, 788–792.
- Stengel, M., 2016. Unified ab initio formulation of flexoelectricity and strain gradient elasticity. *Phys. Rev. B* 93, 245107.
- Stirling, W., 1972. Neutron inelastic scattering study of the lattice dynamics of strontium titanate: harmonic models. *J. Phys. C: Solid State Phys.* 5, 2711–2730.
- Tagantsev, A.K., 1991. Electric polarization in crystals and its response to thermal and elastic perturbations. *Phase Transit.* 35, 119–203.
- Toupin, R.A., 1956. The elastic dielectric. *J. Ration. Mech. Anal.* 5, 849–915.
- Veselago, V.G., 1968. The electrodynamics of substances with simultaneously negative values of ϵ and μ . *Sov. Phys.* 10, 509–514.
- Wang, B., Gu, Y., Zhang, S., Chen, L.-Q., 2019. Flexoelectricity in solids: progress, challenges and perspectives. *Prog. Mater. Sci.*, 100570.
- Wang, Z.-P., Sun, C.T., 2002. Modeling micro-inertia in heterogeneous materials under dynamic loading. *Wave Motion* 36, 437–485.
- Weber, W., 1974. New bond-charge model for the lattice dynamics of diamond-type semiconductors. *Phys. Rev. Lett.* 33, 371–374.
- Weber, W., 1977. Adiabatic bond charge model for the phonons in diamond, Si, Ge, and α -Sn. *Phys. Rev. B* 15, 4789–4803.
- Whitham, G.B., 1974. *Linear and Non-linear Waves*. J. Wiley N.Y.
- Xu, T., Wang, J., Shimada, T., Kitamura, T., 2013. Direct approach for flexoelectricity from first-principles calculations: cases for SrTiO_3 and BaTiO_3 . *J. Phys. Condens. Mater.* 25, 415901.
- Yamada, Y., Shirane, G., 1969. Neutron scattering and nature of the soft optical phonon in SrTiO_3 . *J. Phys. Soc. Jpn.* 26, 396–403.
- Yudin, P.V., Tagantsev, A.K., 2013. Fundamentals of flexoelectricity in solids. *Nanotechnology* 24, 43001.
- Yudin, P.V., Ahluwalia, R., Tagantsev, A.K., 2014. Upper bounds for flexoelectric coefficients in ferroelectrics. *Appl. Phys. Lett.* 104, 082913.
- Zubko, P., Catalan, G., Buckley, A., Welch, P.R.L., Scot, J.F., 2007. Strain gradient induced polarization in SrO_3 single crystals. *Phys. Rev. Lett.* 99, 167601. Erratum: *Phys. Rev. Letters* (2008) 100: 199906.